NASA CR-97-112972

/N 9/-~ R
/24894

SCALING IMPACT-MELT AND CRATER DIMENSIONS:

IMPLICATIONS FOR THE LUNAR CRATERING RECORD

Mark J. Cintala
Code SN4
NASA Johnson Space Center
Houston, TX 77058

and

Richard A.F. Grieve
Geological Survey of Canada
Ottawa, Ontario K1A 0Y3

INTRODUCTION

The consequences of impact on the solid bodies of the solar system are manifest and legion. Although the visible effects on planetary surfaces, such as the Moon's, are the most obvious testimony to the spatial and temporal importance of impacts, less dramatic chemical and petrographic characteristics of materials affected by shock abound (*e.g.*, papers in French and Short, 1968; Roddy *et al.*, 1977). Both the morphologic and petrologic aspects of impact cratering are important in deciphering lunar history, and, ideally, each should complement the other. In practice, however, a gap has persisted in relating large-scale cratering processes to petrologic and geochemical data obtained from lunar samples. While this is due in no small part to the fact that no Apollo mission unambiguously sampled deposits of a large crater (*e.g.*, Rockow and Haskin, 1996; Ryder *et al.*, 1997), it can also be attributed to the general state of our knowledge of cratering phenomena, particularly those accompanying large events.

The most common shock-metamorphosed lunar samples are breccias, but a substantial number are impact-melt rocks (*e.g.*, Stöffler *et al.*, 1980). Indeed, numerous workers have called attention to the importance of impact-melt rocks spanning a wide range of ages in the lunar sample collection (Grieve *et al.*, 1974; Head, 1974b; Dence *et al.*, 1976; Spudis and Ryder, 1981; McKinley *et al.*, 1984; and many others). Photogeologic studies also have demonstrated the widespread occurrence of impact-melt lithologies in and around lunar craters (Howard and Wilshire, 1975; Schultz, 1976; Hawke and Head, 1977b; Spudis, 1978; Wilhelms, 1987, pp.44-53). Thus, it is clear that impact melting has been a fundamental process operating throughout lunar history, at scales ranging from pits formed on individual regolith grains ((McKay *et al.*, 1970)) to the largest impact basins (*e.g.*, Head, 1974a; Wilhelms, 1987, p. 82).

This contribution examines the potential relationship between impact melting on the Moon and the interior morphologies of large craters and peak-ring basins. It then examines some of the implications of impact melting at such large scales for lunar-sample provenance and evolution of the lunar crust.

The Terrestrial Case

The effects of impact melting as a function of event magnitude on Earth have been examined by (Grieve and Pesonen, 1992). The principal results are summarized here as an introduction to a similar approach used below for the Moon.

Because the propagation of shock waves is dependent primarily on the intrinsic properties of the target medium (Gault and Heitowit, 1963; Ahrens and O'Keefe, 1972), the volume of melt and/or vapor generated by an impact is only weakly, if at all, dependent on the gravitational acceleration of the target planet (O'Keefe and Ahrens, 1977). The principal factors governing the volumes of melt and vapor produced by the impact (assuming the most easily modeled case of vertical impact) are the size and properties of the projectile, to which the dimensions of the shocked zones will scale (O'Keefe and Ahrens, 1977), and the impact velocity, which determines the initial shock stress in the impactor and target (*e.g.*, Gault and Heitowit, 1963). Gravity's role is more important, however, in determining the dimensions of the transient cavity (*e.g.*, Chabai, 1965, 1977; Holsapple and Schmidt, 1980, 1982; Schmidt, 1980; Croft, 1983; Schmidt and Housen, 1987) and of the final crater (*e.g.*, Croft, 1985). Specifically, and as described in (Grieve and Pesonen, 1992), this "differential scaling" implies that, relative to smaller impacts, large events will form craters that are smaller relative to the dimensions of the projectile and, therefore, relative to the zone of melting and/or vaporization (Croft, 1983, 1985; Cintala and Grieve, 1984, 1991; Melosh, 1989; Grieve and Cintala, 1991).

This process has manifestations in the terrestrial cratering record. Specifically, when the volume of impact melt V_M as estimated from field observations is plotted against reconstructed transient-cavity diameter D_{tc}, the agreement with previous model predictions (Grieve and Cintala, 1992a) is good (Fig. 1), particularly in light of the effects of erosion. Given the uncertainties in the estimates of the melt volumes and dimensions of the transient-cavity, it is explicitly assumed that the terrestrial data are described well by the model curves.

The expressions used in generating the curves shown in Fig. 1 can also be used to examine parameters such as the depth and volume of melting relative to those of the transient cavity. As increasingly larger events are considered, the zone of melting will extend deeper and will eventually
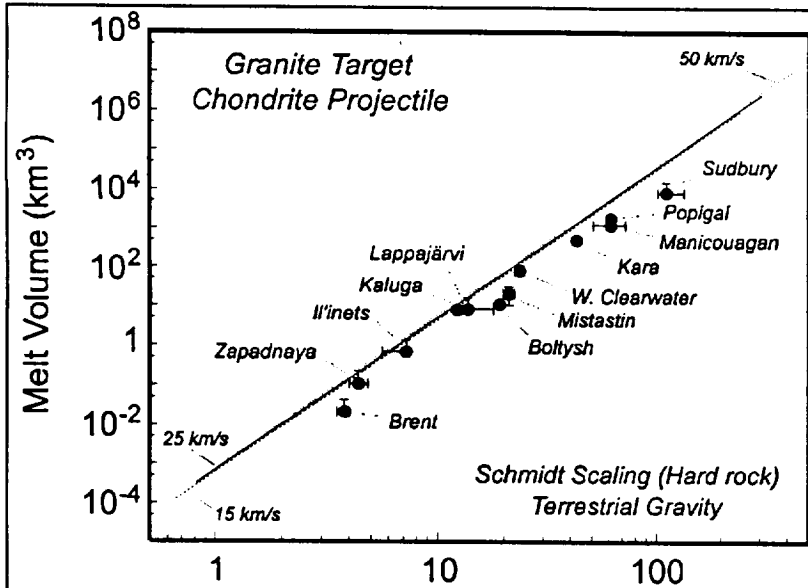
Figure 1. Calculated impact-melt volume as a function of modeled transient-cavity diameter for the terrestrial case of chondritic projectiles and a granitic target (from Grieve and Cintala, 1992). Included are points representing terrestrial craters formed in crystalline rock. Error bars represent estimated uncertainties in melt volumes and cavity dimensions. Note the good agreement with the modeled and actual cases. This figure also shows that the relationship between melt volume and cavity size should be only weakly dependent on impact velocity.

intersect those materials that otherwise would have become the central structures of complex craters. In such cases, however, that portion of the target shocked to levels at or above partial melting could not participate in the formation of the final central peaks, since its internal strength would effectively be zero. Instead, only that part of the central structure outside the limit of melting would remain topographically high. Peak shock-stresses recorded in parautochthonous central-structure materials of terrestrial craters display a trend of increasing recorded stresses until partial melting is reached. In larger craters, the peaks begin to transform into peak rings, but the maximum recorded shock stress remains constant at the level of partial melting (Grieve and Cintala, 1992a). As is obvious from the relative scale of the axes in Fig. 1, these larger craters also contain greater relative volumes of impact melt in their interiors. Ultimately, the very largest impacts would create a volume of impact melt greater than that of the transient cavity, with the final results most likely being a slightly depressed melt pool of considerable dimensions (Croft, 1983; Grieve and Cintala, 1991, 1992a, 1997). Such a melt body would require an extended period of time to crystallize, carrying with it the ramification of potential differentiation processes.

The Lunar Case

The same approach is used here to evaluate the effects of differential scaling under lunar conditions. Three factors yield differences between the lunar and terrestrial cases. First, most large terrestrial impact craters typically form largely in crystalline rocks of granitic composition; their lunar

analogues, at least near the surface, are anorthositic. Second, a given impact will form a larger transient cavity in the weaker lunar gravitational field when compared to its terrestrial counterpart. Finally, typical impact velocities on the Moon will be lower than those on the Earth, owing to its location near the "rim" of the Earth's gravitational potential well. These variations will give rise to substantial differences in the effects of differential scaling on the two planets.

IMPACT MELTING AND LUNAR CRATER MORPHOLOGY

Lunar impact structures exhibit a spectrum of size-dependent morphologies (*e.g.*, Smith and Sanchez, 1973; Howard, 1974; Head, 1976), as are the modes of occurrence of their impact-melt deposits (*e.g.*, Howard and Wilshire, 1975; Hawke and Head, 1977a,b). It might then be expected that some relationship exists between the formation and morphology of various morphological features and the impact-melting process.

Four lunar impact structures have been selected to represent the range of crater morphologies and morphometries. Insofar as there can be wide variations in morphology even within restricted size ranges (*e.g.*, Smith and Sanchez, 1973; Howard, 1974; Cintala *et al.*, 1977), it is difficult to choose a "typical" member of a given size class of lunar craters. With this caveat, the following structures will be treated as broadly representative of their morphologic classes.

Simple craters — The classic "bowl-shape" is typified by the 10-km crater Alfraganus C (Fig. 2). Fresh "bowl-shaped" craters are commonly trapezoidal in profile, with walls possessing nearly constant slopes and small, essentially flat floors. Hummocks and blocks are common on the floors of these craters, but central peaks do not emerge until diameters above 10 km (Smith and Sanchez, 1973; Howard, 1974; Head, 1976). Wall failure is generally limited to small units typically associated with the floor hummocks and to scree emplaced after solidification of the thin impact-melt deposits on the crater floor. Typically, impact-melt deposits visible at simple craters on the Moon occur as thin veneers that cover most of the floor and appear on sections of the rim (Howard and Wilshire, 1975; Hawke and Head, 1977b), where they can be recognized by the cracks along their edges. These veneers can also be detected occasionally by the small concentric craters that indicate formation of a thin regolith on the harder veneer substrate (*e.g.*, Oberbeck
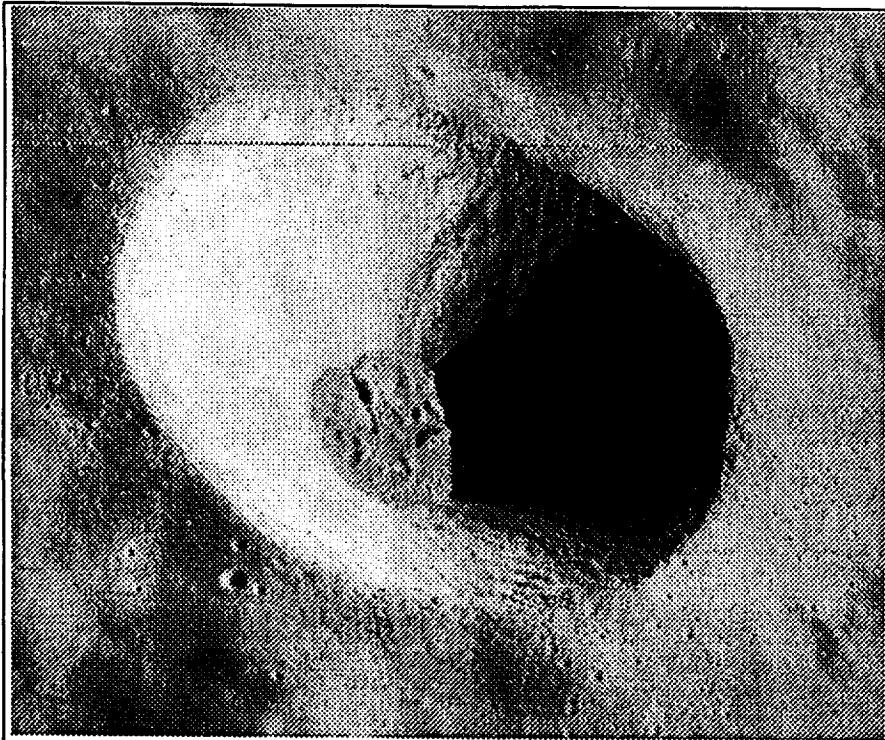
Figure 2. Alfraganus C (10 km in diameter), in the lunar central highlands. This crater is representative of the class of lunar simple craters, which are characterized by smooth walls, relatively flat floors, and large depth/diameter ratios (Portion of Apollo 16 Panoramic Camera Frame 4615).

and Quaide, 1967; Quaide and Oberbeck, 1968). The veneers on the rim often extend partially into the crater, forming smooth patches on the upper wall. Otherwise, the melt formed with such craters has no obvious bearing on the final crater's form. There are examples of simple lunar craters with exterior melt flows (Howard and Wilshire, 1975; Hawke and Head, 1977b) and internal pools on their floors (Howard and Wilshire, 1975; Hawke and Head, 1977a), but they are unusual.

Transitional craters — When viewed in the context of the spectrum of crater morphologies, the transition from simple to complex craters is an abrupt one (*e.g.*, Pike, 1974). Inspection of the individual transitional craters, however, reveals that the changes in morphology are more gradual and less than systematic (*e.g.*, Smith and Sanchez, 1973; Howard, 1974; Head, 1976). Morphological vagaries in this size range tend to cloud the concept of a "typical" transitional crater. Nevertheless, Lalande (Fig. 3) is presented here as being representative of this group. Due to its wide excursions from circularity, its diameter is given as being in the 25-km range.

Lalande displays features that are reminiscent of those in the smaller, simple craters, but it also includes precursors of structures and units that are much better developed in complex craters. Portions of its wall (to the southeast and north, particularly; Fig. 3) show only minor evidence of slumping. Overall, however, Lalande possesses scalloped walls (the "swirl texture" of Smith and Sanchez, 1973) that begin to

exhibit the complexity of the more intricately terraced complex craters. Its central peaks, on the other hand, are only emerging from the floor, and are not the major topographic features characteristic of larger craters. Floor hummocks are more imposing and widespread than those in the simple craters.

Impact-melt veneers occur in the area of the crater's rim as they do in the simple craters, but they are accompanied by leveed flows and occasional, but well-defined, ponds. Gullies and channels are obvious
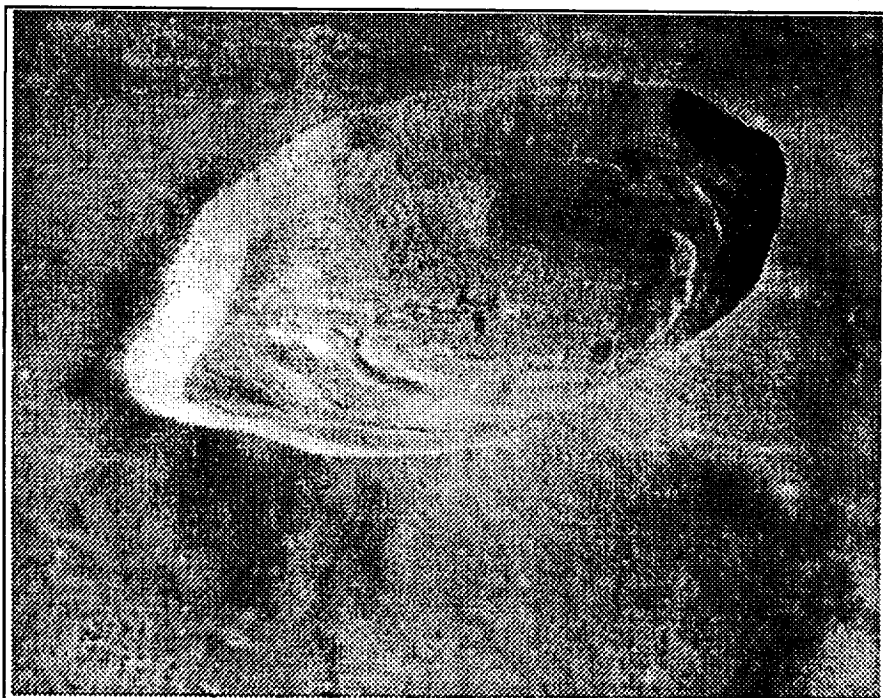

Figure 3. The morphologically transitional crater Lalande (about 25 km in diameter), a few hundred kilometers to the east of the Apollo 14 landing site (Apollo 16 Panoramic Camera Frame 5396).

along the lower walls, particularly in the scalloped areas. They invariably terminate at melt pools and ponds, whether on the floor of the crater or perched between scallops. These gullies are very similar to the features visible in those simple craters that possess distinct melt pools on their floors.

Complex Craters — Full-fledged rebound and wall-failure are well-established in craters the size of Tycho (85 km, Fig. 4). Terraced walls are the rule, as are abundant floor hummocks. A crater of Tycho's size or larger typically possesses a massive central peak or a cluster of peaks (Hale and Head, 1979). The relative heights (Hale and Head, 1979; Pike, 1980; Hale and Grieve, 1982) and volumes (Hale and Head, 1979; Hale and Grieve, 1982) of these peaks increase as a function of size until diameters of about 80 km, after which both values begin to decrease (Hale and Grieve, 1982). Roughly simultaneous with this change, a ring of roughening on the floor, composed of hummocks arranged quasiconcentrically with the central structure, begins to appear (Croft, 1981b; Hale and Grieve, 1982). The relative geometries of these rings are predicted very closely by extrapolating peak-ring vs. rim-crest diameter relationships downward to these crater sizes (Hale and Grieve, 1982). Impact-melt deposits occur at all scales, from the complex

Figure 4. Tycho (85 km in diameter), in the southern lunar highlands. This is a classic complex lunar crater, with the requisite central-peak complex, extensive wall terracing, and omnipresent deposits of impact melt, both in the interior and on the exterior of the crater (Lunar Orbiter V 125M).

sheet on the crater's floor to the thin veneer coating much of the continuous ejecta deposits. Melt pools can be found on the terraces, on the rim, and in hollows in the continuous ejecta. In short, virtually every type of impact-melt deposit can be found in a nearly pristine state at Tycho (Schultz, 1976, pp.228-235).

Peak-Ring Basins — Relatively undegraded peak-ring basins on the Moon are rare, with the freshest of its size being the 320-km Schrödinger (Fig. 5). Interpretation of the interior morphologies of such basins is usually complicated by impact erosion, subsequent volcanic activity, or both. Nevertheless, relevant observations can be made by examining a number of examples; the interested reader is referred to (Wilhelms, 1987) for an exhaustive treatment of the morphology of lunar peak-ring basins.

Peak-ring basins are shallow features for their size. While their depths can be decreased by erosion or externally derived infilling, the fact that details of many interior features (the peak ring and floor hummocks in Schrödinger, for example) are visible indicates that the shallowness is a primary characteristic. Wall terraces are highly developed, and the ratio of floor diameter to rim-crest diameter is somewhat greater than in complex craters (Pike, 1980).

Although these structures have been subjected to more modification than fresh craters such as Tycho, ample evidence remains for extensive interior and exterior deposits of impact melt. Such is the case for Schrödinger between the peak ring and crater wall and in exterior units (Fig. 5), particularly to the basin's east (Hawke and Head,
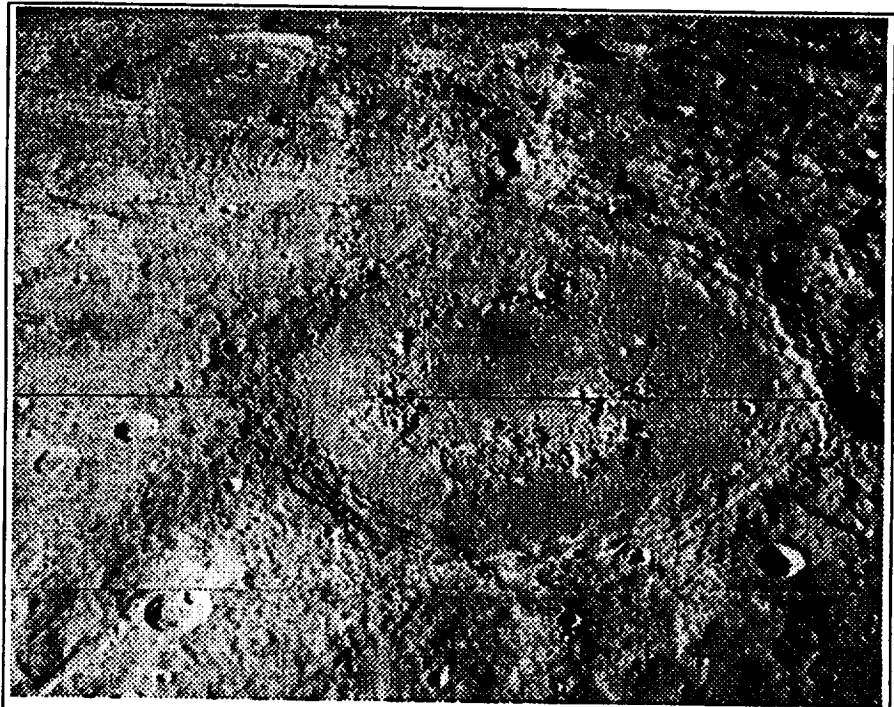

Figure 5. The peak-ring basin Schrödinger (320 km in diameter), near the lunar south pole. Note the fractured floor and the dark-haloed volcanic vent inside the peak ring. This view is to the east-southeast; Antoniadi (140 km in diameter) is the peak-ring basin with the small central peak to the east of Schrödinger. The fresh crater to the north of Schrödinger (just below the framelet boundary bisecting the basin) is the same size as Lalande. (Lunar Orbiter IV 9M)

1977b). Impact melt associated with the larger, multiring impact basins occurs in even greater abundance. Indeed, as has been described in the case of the Orientale Basin by numerous investigators, the volume of impact melt relative to that of the final crater is so great in structures of this size that its presence is ubiquitous, exerting major influence on final basin morphology (e.g., Head, 1974a; Moore et al., 1974; McCauley, 1977; Wilhelms, 1987 pp. 66-77; Spudis, 1993 p. 45 ff).

MODEL APPROACH

Two distinct models are combined in this approach to differential scaling phenomena: one treats the generation of impact melt and vapor, while the other gives the dimensions of the resulting transient cavities and craters. The two will be described briefly, since the melting model (Cintala, 1992; Grieve and Cintala, 1992b) and the crater-scaling relationship (Schmidt and Housen, 1987; Grieve and Cintala, 1992a) have been addressed elsewhere.

Impact Melting and Vaporization

The model for target heating employs a modified Murnaghan equation of state for both the target and projectile materials, each of which is based on the material's linear shock velocity-particle velocity *(U-u)* relationship. The equation of state is given by

$$P = \frac{K_0}{\lambda}\xi(\rho)\left[\left(\frac{\rho}{\rho_0}\right)^{\lambda} - 1\right] + \left(\rho T - \rho_0 T_0\right)\alpha K_0 \tag{1},$$

in which P is the shock stress; K_0 is the bulk modulus; ρ and ρ_0 are the compressed and zero-pressure densities, respectively; T and T_0 are the temperature in the compressed and reference states, respectively; and α is the material's coefficient of thermal expansion. The dimensionless function $\xi(\rho)$ is determined for each material by fitting the Hugoniot as calculated with eq. (1) to the experimentally determined Hugoniot of the material (see Duvall, 1958). The constant λ is derivable from the assumed linear U-u relationship of the material

Table 1. Constants used in thermodynamic descriptions of target and projectile materials. Tahawus anorthosite (McQueen *et al.*, 1967) is used in these calculations, and the "chondrite" is approximated by a dense basalt (Grieve and Cintala, 1992a). C_p is a phase-averaged specific heat. H_m and H_v, and T_m and T_v are the enthalpies and temperatures of melting and vaporization, respectively.

	Anorthosite	"Chondrite"	Iron	H_2O Ice
ρ_0 (g cm^{-3})	2.734	3.580	7.856	0.917
a (cm s^{-1})	2.780×10^5	2.310×10^5	4.269×10^5	1.271×10^5
b	1.536	1.466	1.483	1.580
K_0 (dyn cm^{-2})	2.113×10^{11}	1.910×10^{11}	1.432×10^{12}	1.481×10^{10}
α (K^{-1})	1.324×10^{-5}	1.693×10^{-5}	3.375×10^{-5}	1.125×10^{-4}
C_p (erg g^{-1} K^{-1})	1.389×10^7	1.293×10^7	9.316×10^6	3.550×10^7
H_m (erg g^{-1})	4.264×10^9	4.998×10^9	2.721×10^9	3.355×10^9
H_v (erg g^{-1})	1.065×10^{11}	8.500×10^{10}	6.272×10^{10}	2.269×10^{10}
T_0 (K)	298	298	298	263
T_m (K)	1616.84	1659.94	1809.00	273.15
T_v (K)	3800.00	3800.00	3145.50	372.80

$$U = a + bu \tag{2},$$

in which a and b are material-dependent constants. (Ruoff, 1967) has shown that a good approximation for λ is

$$\lambda = 4b - 1 \tag{3}.$$

K_0 is determined following (Kieffer and Simonds, 1980), who approximated the bulk sound velocity of the material with the coefficient a, giving

$$K_0 = \rho_0 a^2 \tag{4}$$

Phase changes are determined by calculating the entropy increase in the material as a function of shock stress (Duvall, 1958; Ahrens and O'Keefe, 1972). Values for the materials used are listed in Table 1.

Calculations are performed for the normal impact of spherical projectiles into semi-infinite, planar targets. Off-axis decay of the shock front is approximated by assuming that the particle velocity behind the shock decreases in proportion to $Cos^\beta\theta$, where θ is the angle between the axis of penetration to the point of interest, measured at the center of the stress field, and β is the initial ratio of target compression to projectile compression. This approximates the decay in stress toward the target's surface as calculated by more detailed models (*e.g.*, O'Keefe and Ahrens, 1977; Austin *et al.*, 1980; Pierazzo *et al.*, 1997).

Volumes of impact melt and vapor have been calculated for the cases of "chondritic," iron, and H_2O-ice projectiles impacting anorthosite (Fig. 6), where they are plotted as a function of impact velocity. There is little difference between the responses of the anorthosite


Figure 6. Volume of impact melt, vapor, or sum of both for chondritic, iron, and H₂O-ice projectiles as a function of impact velocity. The volumes are expressed in terms of the projectile volume V_p. Included for comparison is the terrestrial case of chondritic projectiles ["Chon"] impacting granite ["Gran"](*cf.* (Grieve and Cintala, 1992a)). Note the strong similarity between the behaviors of the anorthosite and granite in the case of the chondritic projectiles. The lower boundaries of the curves are artificial, in that melting begins at velocities higher than the lowest case treated here (5 km s⁻¹) and lower than the next case (7.5 km s⁻¹). A similar effect occurs for the vapor values.

and granite, indicating that major disparities in behavior between the Moon and the Earth (Grieve and Cintala, 1992a) are not due to the different target materials.

Crater Scaling

The scaling relationship used here to determine the diameter of the transient cavity is that given by (Schmidt and Housen, 1987):

$$D_{tc} = 1.16\left(\frac{\rho_p}{\rho_t}\right)^{\frac{1}{3}} d_p^{0.78} v_i^{0.44} g^{-0.22}$$

(5),

in which D_{tc} is the diameter of the transient cavity; ρ_p and ρ_t are the densities of the projectile and target, respectively; d_p is the diameter of the projectile, v_i is the impact velocity, and g is the gravitational
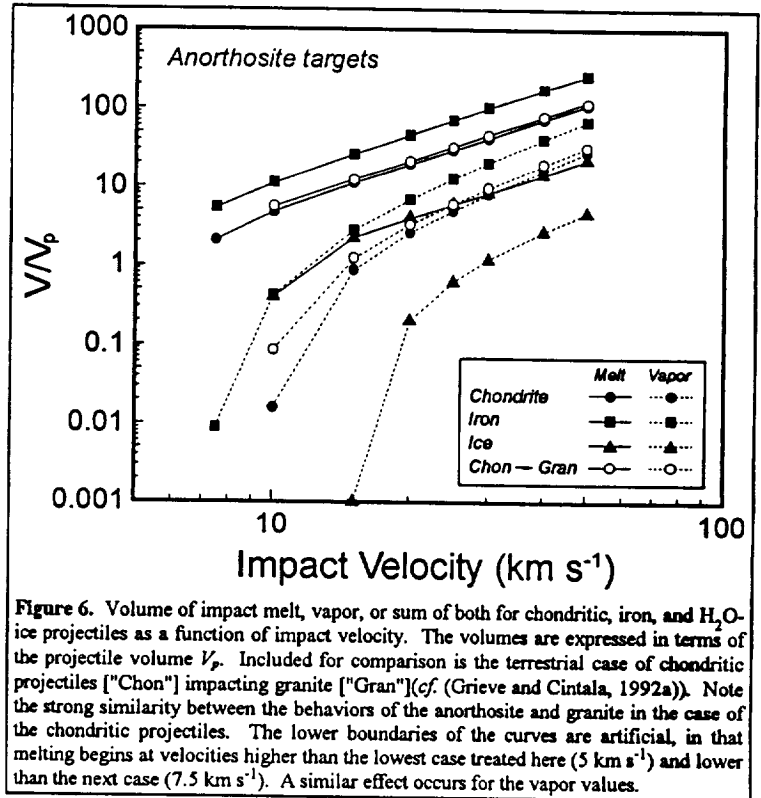
acceleration at the target's surface. Geometric reconstruction of terrestrial craters indicates that a paraboloid of revolution with a depth/diameter ratio of 1:3 is a good approximation of the form of the transient cavity (Dence, 1973; Grieve *et al.*, 1989). Such a geometry is assumed for both the Earth and the Moon.

An actual transient cavity with the geometry as drawn in subsequent figures never exists during the formation of a large crater, due to progressive modification phenomena (*e.g.*, floor rebound, central-structure formation, wall failure, rim collapse, etc.) that occur even as the cavity is growing (Grieve and Robertson, 1979). Wall failure and rim collapse can enlarge a transient cavity significantly. (Croft, 1985) has related the diameter of the final crater to the diameter of the transient cavity, taking into account differences in gravitational acceleration between the planets. Defining D_r to be the final crater diameter (*i.e.*, after modification processes have enlarged the transient cavity) and D_{sc} as the diameter at which the simple-to-complex transition takes place, then the diameter of the final crater can be related to the diameter of the transient cavity as

$$D_r \cong D_{sc}^{-0.18} D_{tc}^{1.18} \tag{6}.$$

This expression holds only for those craters larger than D_{sc} (Croft, 1985); a similar relationship was found by Ivanov (1988).

Equations (5) and (6) can be combined to give

$$D_r = 1.19 D_{sc}^{-0.18} \left(\frac{\rho_p}{\rho_t} \right)^{0.39} d_p^{0.92} v_i^{0.52} g^{-0.26} \tag{7a}.$$

Using a mean simple-to-complex transition diameter of 18.7 km for the Moon (Pike, 1988) yields

$$D_r = 7.03 \times 10^{-2} \left(\frac{\rho_p}{\rho_t} \right)^{0.39} d_p^{0.92} v_i^{0.52} g^{-0.26} \tag{7b}.$$

which is applicable only to complex lunar craters. Equation (7a) can also be arranged to give an expression for d_p, namely

$$d_p = 0.828 D_{sc}^{0.20} \left(\frac{\rho_p}{\rho_t} \right)^{-0.42} D_r^{1.09} v_i^{-0.56} g^{0.28} \tag{7c},$$

which can be used to find the diameter of the projectile responsible for creating a particular final crater.

Relationships between Extent of Melting and Cavity Dimensions

The melt-volume calculations can be combined with eq. (7b) to produce curves relating the volume

of melt to the transient-cavity diameter. The resulting relationships can be described adequately by expressions of the form

$$V_m = cD_{tc}^d \qquad (8),$$

in which c and d are constants determined by the curve-fitting process. Such curves are illustrated in Figure 7 for the cases of chondrite, iron, and H_2O-ice impacting anorthosite targets in a lunar gravity field. The
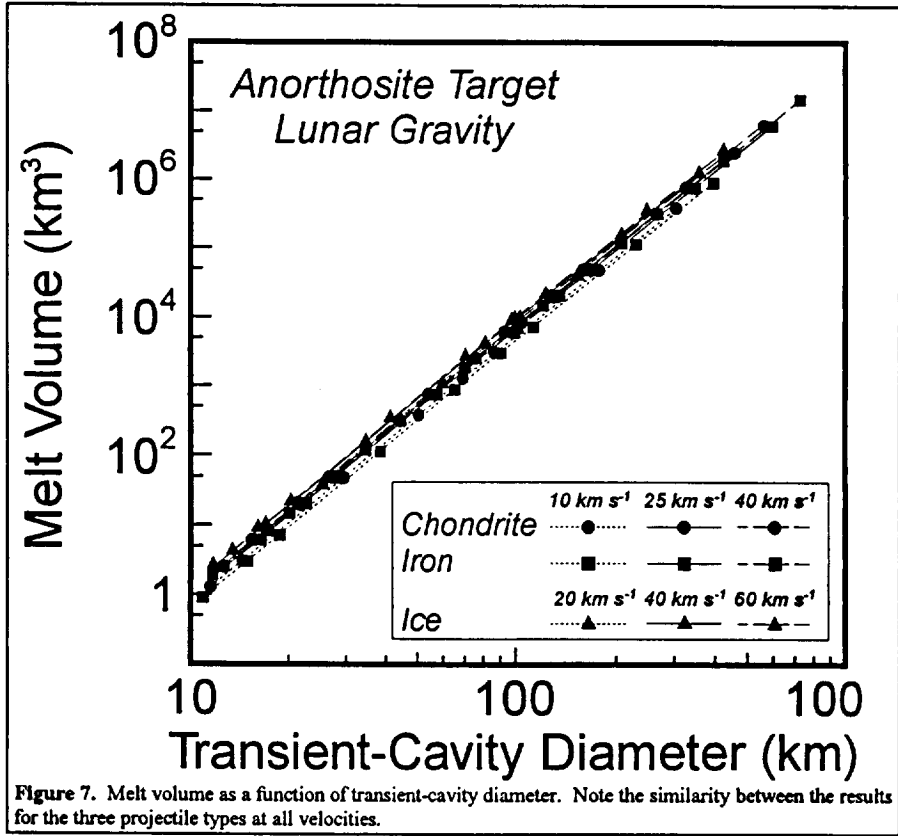
Figure 7. Melt volume as a function of transient-cavity diameter. Note the similarity between the results for the three projectile types at all velocities.

velocities chosen for each projectile type are intended to bracket the probable range of velocities for asteroidal and cometary sources. Constants for the fits used in this figure are given in Table 2.

There is little distinction between the relationships for the different projectiles (Fig. 7). Table 2 shows that the largest difference between two curves in Fig. 7 is slightly more than a factor of 2.3 (iron at 10 km s^{-1} and ice at 60 km s^{-1}). Such differences, in theory, would be sufficient to distinguish between small, fast impactors and large, slow ones (Grieve and Cintala, 1981b), but because of the uncertainties in estimating melt-volumes in actual craters, the differences are so small as to preclude such discrimination in the field. In their study of crater-

Table 2. Constants describing the curves plotted in Figure 7; they are fits of the form given by eq. (8).

Chondrite	c	d
10 km s^{-1}	1.08×10^{-4}	3.85
20 km s^{-1}	1.42×10^{-4}	3.85
40 km s^{-1}	1.67×10^{-4}	3.85
Iron		
10 km s^{-1}	9.08×10^{-5}	3.85
20 km s^{-1}	1.23×10^{-4}	3.85
40 km s^{-1}	1.46×10^{-4}	3.85
H$_2$O Ice		
20 km s^{-1}	1.55×10^{-4}	3.85
40 km s^{-1}	1.88×10^{-4}	3.85
60 km s^{-1}	2.08×10^{-4}	3.85

volumes for a impacts on the Moon and the Earth, showing the two transient cavities scaled to the same size for ease of comparison. The principal causes of the large difference are the greater terrestrial gravitational acceleration and impact velocity, in that order. The effects described above will occur with any crater-scaling relationship, the only difference being the size at which a particular effect takes place.

DIFFERENTIAL SCALING: ANALYTICAL ASPECTS

It is clear that the manifestations of melting become more abundant, obvious, and important as larger impact structures are considered. From this, it can be inferred that the role of impact melting in the cratering process must grow with increasing magnitude of the event. This section addresses a selection of such possible effects, particularly as they bear on the interior morphologies of lunar craters. To do this, a point of reference is required to relate the geometry of the melt zone to that of either the transient cavity or the final crater. Because both occur early in the cratering process, the generation of impact melt and the formation of the transient cavity are intimately connected; we have chosen to use the dimensions of the transient cavity as referents — most often its depth or volume (Grieve and Cintala, 1992a). By virtue of its very nature (*e.g.*, Grieve, 1980; Melosh, 1989, p.76-78), the transient cavity of a large crater is never observed. We believe, however, that there is ample justification for the geometry used here and in (Grieve and Cintala, 1992a). In any case, it is important to maintain a consistent basis for comparison; having established such a basis, adjustments to accommodate other preferred geometries can be made.

Depth of Melting

While the model does not provide information on material trajectories in the target, it does afford the maximum depth at which a particular phase change will occur for a given impactor and impact velocity. For example, depths of melting are plotted in Figure 10 relative to the transient-cavity depth d_{tc} as a function of transient-cavity diameter. (In this and the other sections below, "melting" refers to the onset of fusion.) The most immediate feature of this figure is the dependence of the relative depth of melting on the size of the transient cavity. At 20 km s^{-1}, for example, the maximum depth of melting is only about 15% of the depth of a 1-km transient cavity, but it increases to 50% of the depth for a 50-km cavity. At multiring

basin scales, the depth of melting will exceed the maximum depth of the transient cavity. The relative depth of melting increases with velocity, although the rate at which it grows declines with increasing velocity. This dependence on velocity is weaker than the dependence on the magnitude of the event. There is also a notable effect due to projectile type, with melting by denser impactors restricted to shallower depths relative to the dimensions of the transient cavity, in qualitative agreement with the results of (Kieffer and Simonds, 1980). The maximum difference in the depth of melting is about 30%, and occurs between ice impactors at 60 km s^{-1} and iron at 10 km s^{-1}.
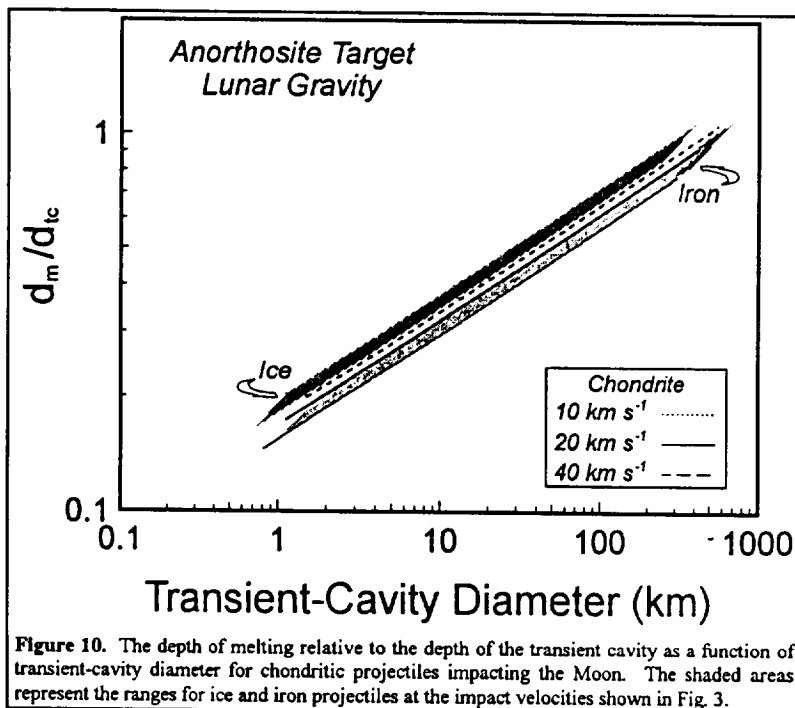
Figure 10. The depth of melting relative to the depth of the transient cavity as a function of transient-cavity diameter for chondritic projectiles impacting the Moon. The shaded areas represent the ranges for ice and iron projectiles at the impact velocities shown in Fig. 3.

If the relative maximum depth of excavation were isometric with increasing transient-cavity diameter, it would appear as a straight line parallel to the horizontal axis. In such a case, the maximum depth of melting would increase relative to the maximum depth of excavation, implying that the depth of melting would, at some point, exceed the depth of origin of ejecta. The potential implications of this effect will be addressed in a later section.

Another aspect of Fig. 10 concerns central peaks. If target material at depth were melted by the impact, then that material could not be part of a central peak's structure in the resulting final crater form (Grieve and Cintala, 1992a). Specifically, the depth of melting in such a case would define the minimum depth of origin of the top of the central peak or peaks. This topic will also be discussed later.

Volume of Melting

The volume of impact melt changes relative to the size of the transient cavity (Fig. 11). As in the case of the relative depth of melting, the magnitude of the impact event is the dominant factor, followed by secondary effects due to impact velocity and projectile density. The curves in this plot are very similar to those for the depth of melting (Fig. 10), although the slopes are different. Nevertheless, the descriptions of the relationships and controlling variables given in reference to Fig. 10 are also applicable to the volume of melting.

In the case of the chondritic projectiles, the range of impact velocities considered here can account for a difference in melt volume of about 30% for a transient cavity of a given size. Figure 11 illustrates that this velocity dependence is smallest for ice, and greatest for iron. Given a specific transient-cavity diameter, the maximum variation in the relative volume of melt would be between the fastest ice impactor considered here (60 km s^{-1}) and the slowest iron (10 km s^{-1}), amounting to a factor of about 2.5.

The overall trend of increasing relative melt volume is consistent with the observations of lunar craters summarized earlier: growing evidence of impact melt is correlated with increasing crater size. It is apparent
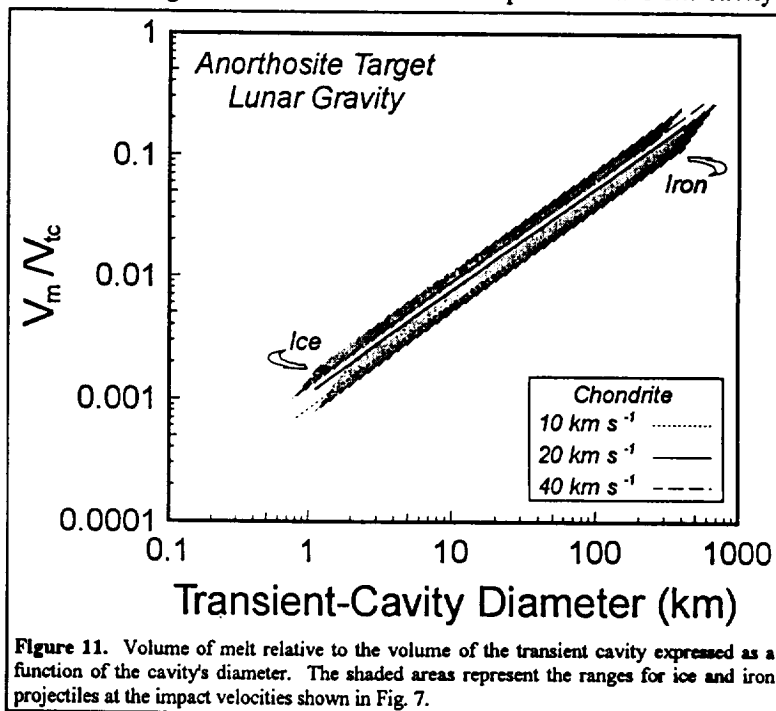

Figure 11. Volume of melt relative to the volume of the transient cavity expressed as a function of the cavity's diameter. The shaded areas represent the ranges for ice and iron projectiles at the impact velocities shown in Fig. 7.

from Fig. 11 that, unless some unforeseen process takes effect, the volume of melt will exceed that of the excavated material, and even that of the transient cavity, at finite cavity diameters. This was addressed by (Grieve and Cintala, 1992a) for impacts on Earth. A volume of melt equal to the transient cavity's volume would occur on the Moon at a cavity diameter approaching the diameter of the Moon, if such a thing is

possible on a spherical target. This would approach a whole-Moon melting event, a class of impacts that is treated in detail by (Tonks and Melosh, 1992, 1993).

GEOMETRIC EFFECTS ON CRATER FORMS

The depth and volume of melting form the basis for many of the effects that differential scaling can have on the size-dependence of the lunar cratering record. This section describes the basic geometric relationships between the transient cavity and the melt zone for each of the four craters selected earlier as examples.

Simple craters — The melt zones of simple craters represent only a small fraction of the transient cavity's volume (Fig. 12). In the case of Alfraganus C, the volume ratio of melt to transient cavity is about 0.007.

Figure 12. Schematic, cross-sectional diagram of the idealized configuration of the transient cavity (left) and the present crater (right) for the case of Alfraganus C. In this and the subsequent three figures, D_{tc}, D_f, and D_p represent the diameters of the transient-cavity, the final crater, and the projectile, respectively.

While a portion of melt remains within the crater, this volume is typically so small relative to the volume of the final structure that it can have only a minimal effect on the crater's morphology and morphometry. The general observed scarcity of flow features implies that these melts solidified relatively quickly, were not thick enough to generate sufficient shear stresses to cause flow, or both. Simple terrestrial craters such as Brent (Grieve and Cintala, 1981a) possess melt lenses that have been buried under subfloor breccias emplaced by wall failure; the lunar case is probably similar.

Transitional craters — While the relative amount of melt created at Lalande, with a melt to transient-cavity volume ratio of only 0.015, is twice that of Alfraganus C, it still does not represent a significant portion of the transient cavity's volume (Fig. 13). The obvious question arises: if craters such as Lalande (and larger) display such extensive wall failure and, therefore, a much more active and complex
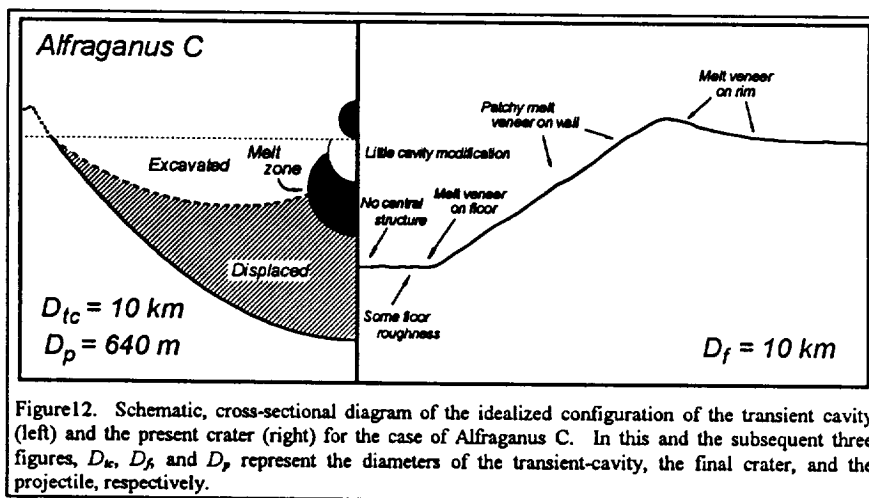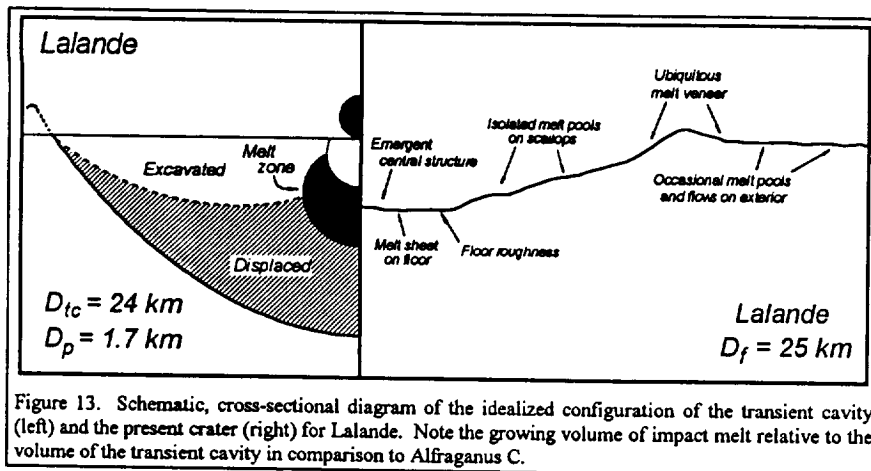
Figure 13. Schematic, cross-sectional diagram of the idealized configuration of the transient cavity (left) and the present crater (right) for Lalande. Note the growing volume of impact melt relative to the volume of the transient cavity in comparison to Alfraganus C.

modification pattern, why are their impact-melt deposits so much more obvious than those of smaller, simple craters? A partial answer lies in the increasing relative volume of impact melt and the intensity of cavity modification (Fig. 13).

Studies of simple terrestrial craters show that their subfloor breccia lenses are chaotic deposits (*e.g.*, Shoemaker, 1963; Grieve and Cintala, 1981a), indicating that the slope failure associated with cavity readjustment is not an orderly process. It is not difficult to envision a thin coating of impact melt in a steep-walled, simple crater being incorporated into the slumped material during its chaotic emplacement at the bottom of the cavity (*e.g.*, Grieve *et al.*, 1977; Melosh, 1989). The situation is more complicated in the larger craters, however, in terms of both scale and phenomenology. Above all, more impact melt is generated and remains within the cavity, and it simply becomes more difficult to hide. The scale and style of the cavity-modification processes also contribute to the greater visibility of the melt deposits in larger craters. Wall failure in larger craters takes place on a much greater scale; slumping occurs in units that are considerably more coherent and slide into the interior of the crater *en masse* (*e.g.*, Mackin, 1969; Grieve *et al.*, 1977; Settle and Head, 1979; Melosh, 1989, Chap. 8). In this process, the gross stratigraphy of the wall materials remains relatively intact, ensuring that most of the melt deposits will stay on top.

Complex Craters — Even a cursory comparison of Lalande and Tycho (*cf.* Figs. 3 and 4) indicates that impact melting is a much more obvious and important process in the formation of larger craters. With a volume ratio of almost 0.04, the amount of impact melt has become a considerable fraction of the transient cavity's volume (Fig. 14). The melt zone extends well into the axial region of the displaced portion of the transient cavity, which is the volume that would take part in central-peak formation.

It is important to remember that the calculations used here were performed for vertical impacts of spherical projectiles into homogeneous targets. While projectile shape plays only a moderate role in controlling cratering
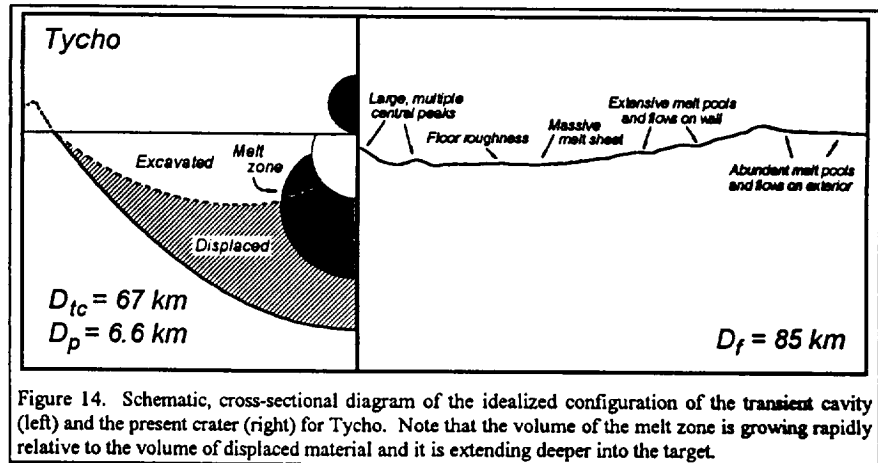

Figure 14. Schematic, cross-sectional diagram of the idealized configuration of the transient cavity (left) and the present crater (right) for Tycho. Note that the volume of the melt zone is growing rapidly relative to the volume of displaced material and it is extending deeper into the target.

phenomenology (*e.g.*, Holsapple and Schmidt, 1987; Schultz, 1988), the impact angle and target structure also have implications for the propagation of the shock front and its subsequent effects. Impact angle will influence the downrange motion of the impact melt and produce an offset in the center of rebound. Irregularities in the physical structure of the target will be reflected in the boundary between melted and unmelted material. It is likely that large-scale inhomogeneities in the target will affect the morphology of the final rebounded mass, resulting, for example, in multiple central peaks instead of a single central mass.

Peak-Ring Basins — Almost a tenth of the volume of Schrödinger's transient cavity was impact melt. As rebound and other modifying effects severely reduce the volume of the transient cavity, they enhance the relative importance of the melted volume. Indeed, a large portion of the displaced and rebounding volume itself is melt, and must be considered an important agent in accounting for the interior morphology of peak-ring and larger basins.
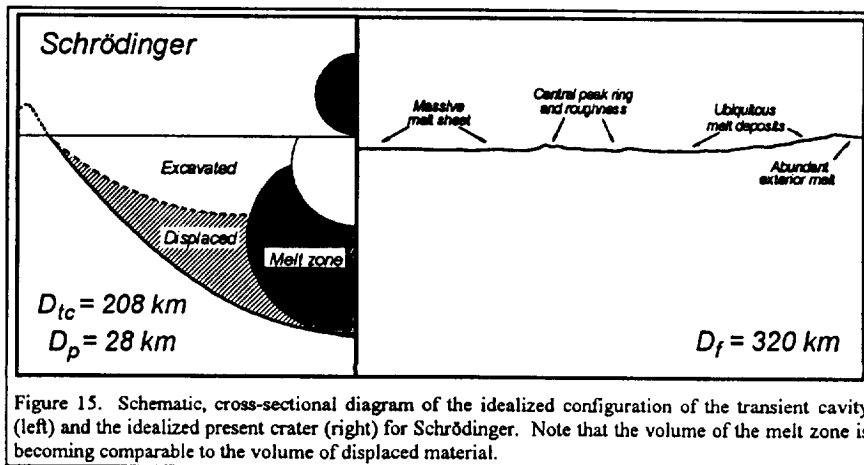
Figure 15. Schematic, cross-sectional diagram of the idealized configuration of the transient cavity (left) and the idealized present crater (right) for Schrödinger. Note that the volume of the melt zone is becoming comparable to the volume of displaced material.

In the model calculation for Schrödinger, the deepest part of the melt zone actually surpasses the base of the transient cavity (Fig. 15) and would penetrate even deeper in larger impacts. Use of eq. (9b; see below) to

estimate the current volume of Schrödinger gives 1.46×10^5 km^3, while the calculated total melt volume is 1.09×10^5 km^3, fully 75% of the visible volume of Schrödinger.

In the case of Schrödinger, the molten portion of the displaced volume will, in the compressed state, behave similarly to the solid portion of the displaced volume. Even during the early stages of cavity readjustment, as its density and hence specific inertia will differ little from the surrounding solid material, the role played by the melt will be indistinguishable from that of the solids (O'Keefe and Ahrens, 1996). The distinction between the melt and solids will emerge near the end of the impact event, however, when the melt's inability to support itself topographically becomes important.

DYNAMIC EFFECTS ON PROCESSES AND MORPHOLOGIES

The effects of these changes in relative cavity and melt geometries with event size are observable in the lunar cratering record. This section will address some of the specific consequences of the differential-scaling hypothesis and relate them to observations of lunar craters and basins.

Ejection of Impact Melt

It has long been recognized that the relative volume of impact melt remaining inside the final crater increases with crater size. (Dence, 1971) and (Grieve et al., 1977) attributed this tendency to the decrease in excavation efficiency as cratering events grow in magnitude. When coupled with a demarcation between ejected and displaced material, the calculations outlined above can be used to estimate the efficiency of impact-melt ejection as a function of crater size.

The z-model of (Maxwell, 1973, 1977) can be used to approximate the boundary between ejected melt and the portion that is simply displaced and thus retained in the crater. Figure 9 illustrates two examples of such a delineation, in which the hinge streamline divides the melted zone into an ejected volume and a displaced volume that remains within the transient cavity. The two volumes can be calculated after fitting a curve (a partial limaçon of Pascal) to the profile of the melt zone. The volume between the hinge streamline and the limit of melting can then be found by integration, since the geometry is axially symmetric under the modeled condition of normal impact. After the amount of melt remaining within the crater is determined, it is a simple matter to calculate the ejected volume.

The shape of the hinge streamline is dependent on the value of z used in describing the flow field. A value of 2 will yield a purely radial flow field; larger values of z will produce greater curvature of the streamlines and higher angles of ejection as measured at and from the surface of the target (Maxwell, 1973, 1977). Although the z-model appears to be suited to the analysis of smaller craters (Croft, 1980; Grieve *et al.*, 1989), previous attempts to apply the z-model to observations of large terrestrial craters have met with only limited success (Hörz *et al.*, 1983; Redeker and Stöffler, 1988). In particular, simultaneous matching of depths of excavation and transient-cavity radii with a single value of z has been difficult. As summarized by Grieve (1988), this could be due either to misinterpretation of the constraining observations or to deficiencies in the z-model as applied at the scales of complex terrestrial craters. Therefore, all results from the z-model presented here are first-order values only, and they could be subject to revision when more detailed representations of the flow field become available.

Figure 16 illustrates an example of the relationship between the exponent z and the relative volumes of displaced and ejected melt. Larger values of z describe streamlines that excavate deeper material, hence ejecting larger fractions of the impact melt. Attempts at applying the z-model with constant z to terrestrial craters, however, indicate that values of z approaching 2.9 do not appear to be the case, as such streamlines cause ejection of material from levels too deep to be consistent with observations at the Ries (Hörz *et al.*, 1983) and Haughton (Grieve, 1988) structures. In the case of the Ries crater, on the other hand, values

Figure 16. The effects of changing values of z on the fraction of melt retained inside and ejected from lunar transient cavities of different diameters.
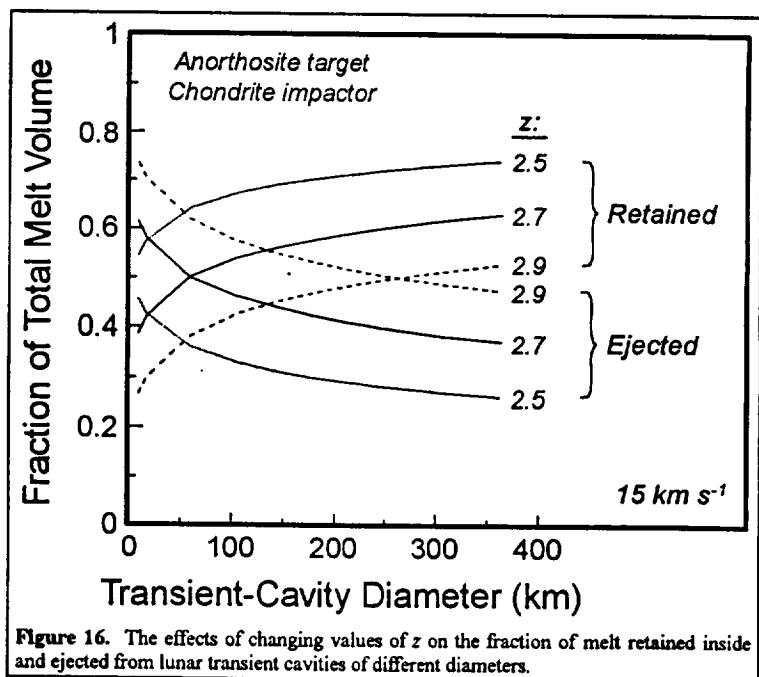
of z smaller than about 2.7 do not produce sufficiently deep excavation. It must be added, however, that neither does a value of 2.7 accommodate the observations perfectly, in that excavation is still too deep when the other Ries constraints of diameter and total volume of ejecta are met (Hörz *et al.*, 1983). Insofar

as higher and lower values of z produce even greater disagreements, however, a value of 2.7 is taken here as a reasonable compromise.

The effects of size-dependence in the volume of melt ejected can be examined via the four representative lunar craters. The third column in Table 3 gives the total volume of melt generated as a fraction of the transient cavity's volume. When the calculated fraction of non-ejected melt f_{non} is applied to this value, the relative volume remaining in the crater is the result, given in the fifth column. The last two columns of the table take the two relative volumes of melt for each of the four craters and divide them by the equivalent number for Alfraganus C. The sixth

Table 3. Melt-related parameters for the four lunar craters used as examples in the text. The superscripts *tot* and *non* refer to the entire volume and non-ejected fraction of impact melt, respectively, while *Alf* implies that the value is given relative to that for Alfraganus C. The column labeled "f_{non}" is the calculated fraction of the entire melt volume that is not ejected from the transient cavity. These values assume a lunar impact velocity of 16.1 km s^{-1}

	D_r (km)	D_{tc} (km)	V_m^{tot}/V_{tc}	f_{non}	V_m^{non}/V_{tc}	$(V_m^{tot}/V_{tc})_{Alf}$	$(V_m^{non}/V_{tc})_{Alf}$
Alfraganus C	10	10.0	7.05×10^{-3}	0.391	2.76×10^{-3}	1.00	1.00
Lalande	25	23.9	1.48×10^{-2}	0.445	6.59×10^{-3}	2.10	2.39
Tycho	85	67.5	3.58×10^{-2}	0.514	1.84×10^{-2}	5.07	6.67
Schrödinger	320	207.6	9.29×10^{-2}	0.594	5.52×10^{-2}	13.17	20.01

column provides this value for the entire melt volume, while the last column gives this value only for that volume of melt remaining in the crater. Ejection of melt from the cavity obviously leaves less melt inside the crater (compare the fourth and sixth columns), but it increases the relative difference between the smallest and largest craters (compare the sixth and seventh columns). Indeed, by taking the ejection of impact melt into account, the relative difference in melt volume contained in Alfraganus C and Schrödinger increases by a further 50%. This is important, but secondary to the original difference between the two, which is due simply to the effects of differential scaling.

The Size Dependence of the Morphology of Impact-Melt Deposits

In their description of the changing morphology of impact-melt deposits inside lunar craters as a function of crater size, (Hawke and Head, 1977a) noted that "...An important question is why melt deposits are generally not observed on the interiors of small craters." Figure 12 shows that the relative volume of melt formed in small craters is a minor fraction of the cavity's volume — only about 0.007 V_{tc} in the case of a 10 km cavity (assuming an impact velocity of 16.1 km s^{-1}) and even less for smaller ones. Insofar as much of this melt should be ejected from craters in this size range (*e.g.*, Orphal *et al.*, 1980; Fig. 12 and

Table 3), little evidence of interior melt should exist, particularly if the slumping and burial mechanisms described by (Hawke and Head, 1977b), for example, were also active.

Lalande possessed a transient cavity with a diameter only slightly smaller than that of the final crater. When melt ejection is taken into account, a 24 km transient cavity would have had a relative volume of melt 2.4 times larger than that for one the size of Alfraganus C (Table 3). In a comparison of these two craters (Figs. 2 and 3), however, even this small difference in melt volume is obvious in both the interior and exterior deposits. Melt flows at Lalande are apparent on the rim, between and on terraces, and on the floor. While this increase in melt volume is not a major influence on crater morphometry, it is obvious that impact melting at this scale is more important than in the simple-crater case.

The maximum diameter attained by Tycho's transient cavity would have been about 68 km. Allowing for ejection, the relative volume of melt remaining in the crater would have been almost 3 times more than that in Lalande (7 times more than that in Alfraganus C; Table 3). The effect of such a small difference in relative melt volume on the morphological importance of the deposits, both inside and outside the crater, is dramatic. There is also more evidence that the melt remained fluid for a longer period than in Lalande. Flows are ubiquitous, cooling cracks are visible almost everywhere on the crater floor, and many ponds in the crater's ejecta deposits appear to have been liquid long enough to solidify with flat surfaces, including cooling cracks in some instances (Howard and Wilshire, 1975).

Schrödinger would have had a transient cavity about 208 km in diameter, with a relative volume of non-ejected melt 3 times greater than at Tycho (20 times more than in Alfraganus C; Table 3). Even if the retention effect due to size were not as effective as implied by Table 3, it is hardly extreme to suggest that much, if not most, of the smooth, higher albedo facies inside the basin, as well as in its near-field exterior deposits, is impact melt.

This effect of the relative increase in the volume of melt deposits with crater size can be approached in a slightly different way. The internal volumes of the final craters (that is, the craters after rebound, wall failure, and other modification phenomena) can be estimated with Croft's (1977) observational relationship

$$V_i = 0.040 D_R^{3.00} \tag{9a}$$

for craters smaller than 13 km, and

$$V_i = 0.238 D_R^{2.31}$$ (9b)

for craters between 19 and 150 km in diameter. As Croft extrapolates eq. (9b) to diameters larger than 150 km with reasonable results, the same will be done here. Eqs. (9a and b) were fit by Croft to observed crater volumes, and therefore include the volume occupied by the interior deposits of impact melt. The volumes of these interior melt deposits are assumed here to equal the non-ejected volume of melt as calculated above. Thus, the final crater volume when the impact-melt component is taken into account V_f will be given by

$$V_f = V_i + V_m^{non}$$ (10).

Knowing V_i from eqs. (9) and V_m^{non} from the method used above, the volume of impact melt retained relative to V_f can then be determined for each of the four craters. (Assuming that the shapes of the craters below the melt are similar, which might well not be the case, particularly for Schrödinger.) Using this approach, Lalande had about 3, Tycho about 11, and Schrödinger about 34 times more impact melt retained relative to the final crater volume than did Alfraganus C.

The Relationship between Cavity Size and Relative Clast Content of Impact Melt

Impact-melt rocks in the Apollo collection range from fragmental breccias with only minor evidence of melting to clast-free impact-melt rocks. By analogy with terrestrial rocks, the latter are considered to be samples of coherent impact-melt sheets, while the former originated in a region of lower shock stress (*e.g.*, Simonds *et al.*, 1976a, b). Clast-free melt rocks, however, are rare in the lunar-sample collection (Taylor *et al.*, 1991). While it is impossible to make a quantitative comparison because of vastly different sampling environments, a substantial proportion of known terrestrial impact-melt rocks is relatively clast-poor, particularly at craters comparable in size to the lunar structures considered above.

The models used here provide a qualitative means of estimating the relative clast abundances in lunar impact melts. The basic tenet of this estimate lies in the configuration of the impact melt during the excavation stage of the cratering event. Specifically, it is assumed that the non-ejected volume of impact melt lines the idealized, paraboloidal transient cavity of surface area A_{tc}, much in the way first described by

(Dence, 1971) and as predicted in the calculations of (O'Keefe and Ahrens, 1993). The quantity V_m^{non}/A_{tc} will yield the thickness of the melt lining, which, for ease of calculation, is assumed to be of uniform thickness at all points along the surface of the cavity. (This modeled thickness is relative to the *maximum*

Figure 17. The effective thickness of the melt lining the idealized transient cavity as a function of the final crater diameter. The curves for the iron and ice projectiles would be very similar to those shown here for the chondrite, with little vertical displacement between the three groups of curves. The values for the four lunar craters used as examples in the text are indicated on the vertical axis.

dimensions of the transient cavity; at any earlier time, the melt lining would be thicker in direct proportion to both the smaller surface area of the cavity and the volume of melt still inside the cavity.) Values for this effective melt-lining thickness are illustrated in Figure 17. It is not critical that this assumed geometry be correct to derive a sense of how the nature of impact-melt rocks might change with cavity size.

In the case of smaller craters, a greater opportunity will exist for the entire volume of a thin melt layer to interact with the clastic debris lining the cavity wall, thus permitting the melt to incorporate a greater volume of clasts. At some sufficiently small thickness, the melt will become choked with clasts, cooling rapidly in its travel up the wall of the growing cavity. The melt lining of Alfraganus C, for example, would have been just over three meters thick (using the assumed impact velocity of 16.1 km s⁻¹). A sheet three meters thick, having to travel kilometers from its point of origin to approach the rim of the cavity, would mix with clastic debris from the wall of the growing crater to the extent that little clast-free liquid would remain. As would be expected, there is little evidence of melt deposition in or around this crater or others of its size.

The transient cavity of Lalande, being somewhat larger and therefore possessing a greater initial ratio of melt volume to cavity volume, would have had a lining almost 20 meters thick. Although this is not particularly imposing, it apparently was sufficient to produce both interior and exterior flows, as well as pools on the interior terraces and a notable sheet on the crater's floor. As catalogued by (Hawke and Head,

1977b), the main concentration of exterior impact melt is on the northeastern rim, opposite the region of maximum slumping in the crater. Low-sun photographs, however, reveal numerous, higher-albedo, flow-like deposits on the southern rim and at other locations around the crater. There are incipient analogues of these features on the rim of Alfraganus C in a sector extending roughly from the south to the southwest. The appearance of these units around Lalande and in a similar, though less-developed, manifestation on the rim of the smaller crater are consistent with this view of clast-laden impact melts.

The transient-cavity of Tycho would have had a melt lining more than 150 meters thick, sufficient to produce abundant exterior flows and deposits, as well as a highly developed and morphologically complex interior melt sheet. In the cases of such large craters, it is important to note that the volume — and therefore the interior surface area — decreased dramatically during the modification of the transient cavity. In the process, if ejection of melt from the cavity did not keep pace with rebound, the relative thickness of the melt lining would increase, with results like those observed in Tycho.

The thickness of the melt lining in Schrödinger would have exceeded 1.4 kilometers. Unless irregularities in the cavity wall occurred on the same scale to induce turbulence, it is difficult to imagine a way in which clasts could be incorporated efficiently into and disseminated throughout such a massive volume of impact melt. It has been suggested that impact-melt inside large terrestrial craters was highly inviscid due to its superheated nature and possibly to the incorporation of shock-vaporized materials (Floran *et al.*, 1978; Grieve and Floran, 1978). Turbulence would then be encouraged in an environment characterized by high shear gradients, large vorticities, and other agents of mixing, leading in turn to the incorporation of clastic debris into the melt. It is likely, however, that much of this debris would be absorbed because the melt's mean temperature would be well above the solidus of any reasonable lunar material, and its thermal inertia would be very high by virtue of its great mass, so it would cool slowly.

Simonds *et al.* (1978) and Floran *et al.* (1978) studied impact melts at the 100-km diameter Manicouagan terrestrial impact structure. They found that much of its melt sheet is clast-free and that its original thickness was roughly 500 m. If the calculated amount of nonejected melt pooled at the bottom of Schrödinger (assuming a flat-floor geometry below the melt), it would be more than 3.5 km thick. This would take much longer to cool and would possess a much greater thermal mass to provide energy for

digestion of clasts than Manicouagan had (*cf.* Grieve *et al.*, 1991). Indeed, without making too much of this approximate calculation, this is a kilometer thicker than the Sudbury Igneous Complex, a highly differentiated body (Naldrett and Hewins, 1984) that is believed to represent the remnant of the impact-melt sheet at the Sudbury impact structure (originally 200-250 km in diameter; Grieve *et al.*, 1991; Stöffler, 1994).

The Role of Impact Melting in the Progression from Simple Craters to Peak-Ring Basins

The upper two panes in Figure 18 represent a simplified view of the regions of formation of impact melt, the volumes of ejected and displaced material, and the streamlines resulting from the z-model (with z=2.7) at Alfraganus C and Tycho. The hinge streamline (Croft, 1981b) divides the ejected material from
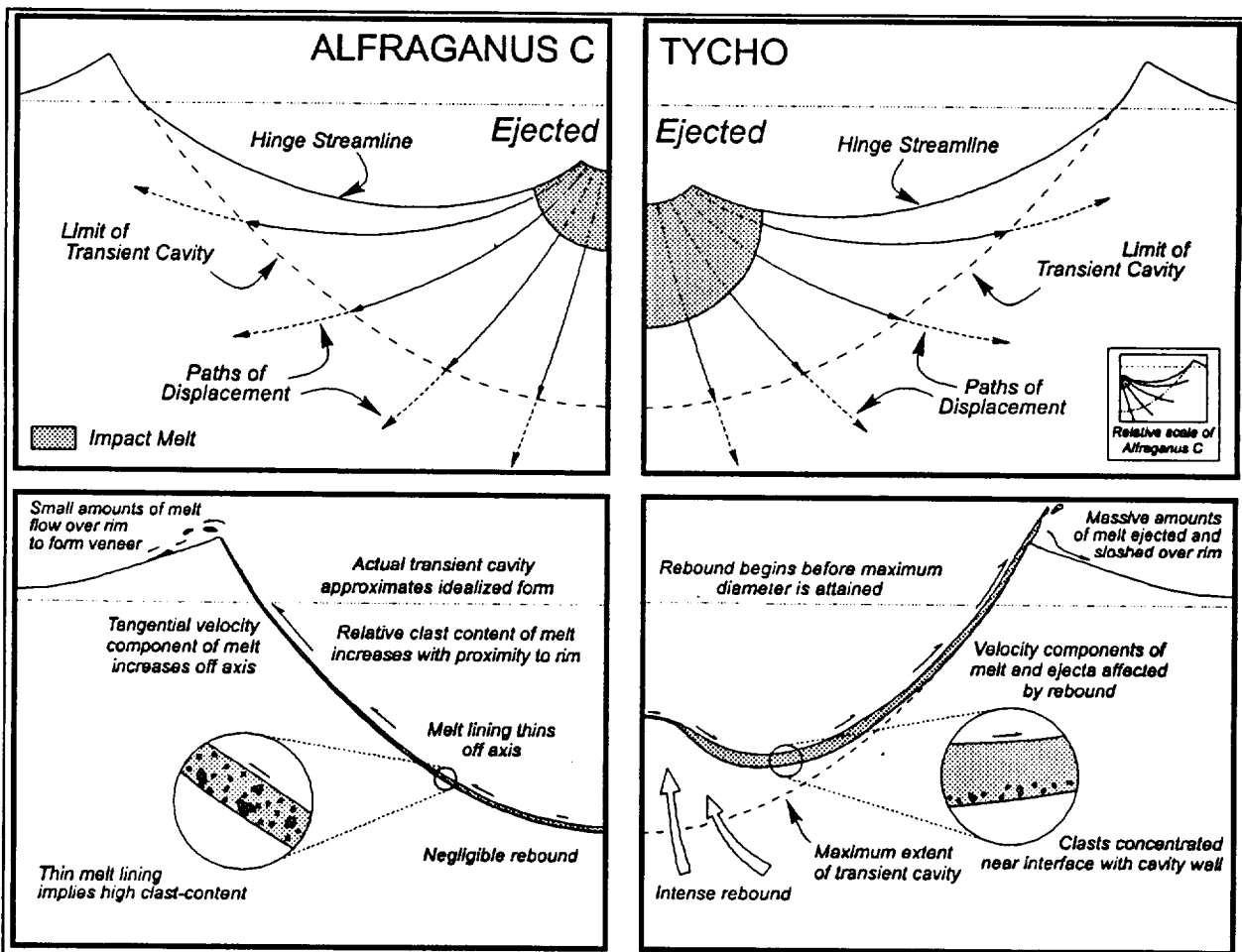
Figure 18. Schematic illustration of the differences between the formational configurations of simple (left, represented by Alfraganus C) and complex craters (right, exemplified by Tycho). The transient cavities are shown as being the same size for ease of comparison. In reality, the entire volume shown in the upper-left pane would fit inside the melt zone of Tycho. (See the inset in the upper-right pane for an indication of the actual difference in scale between the two cavities.) Details of this figure are described in the text.

the displaced material, which is driven downward and outward by the shock and rarefaction process. This mechanism is responsible for the structural component of the cavity's rim (Croft, 1981a) and, in the case of simple craters, much of the final crater's volume. The z-model is assumed explicitly to apply only in the case of incompressible flow. Incompressible flow takes place well after formation of the impact melt, which occurs during the early stages of the cratering process (*e.g.*, O'Keefe and Ahrens, 1977). Figure 18 does not violate the z-model's assumption, however, since it merely maps the original location of the melt by superimposing it on the paths that the displaced material takes during the later stages of the cratering event.

Also included in Figure 18 are the limits of the transient cavities, which are in keeping with the assumption of constant cavity geometry. The relative difference in displaced volume between the two cavities is not great, but much of that volume is occupied by impact melt in the case of Tycho. This combination of greatly different melt volumes and similar cavity geometries gives rise to the thinner melt linings in the case of simple craters. In the case of the near-axial streamlines, a fairly large volume of melt will be spread over a fairly small section of the growing cavity. The streamlines farther off-axis will carry smaller volumes of melt farther from their locations of formation, to be spread over an increasingly larger area of the cavity. This will produce a melt layer, at least for the time that this flow pattern is followed, that thins the cavity's rim is approached. This is illustrated in the bottom panes, along with the fact that the thinner melt will also have higher absolute velocities tangential to the cavity's surface. A gradient in clast content is thus would be established, with the thinner melt closer to the rim being both the most clast-rich and ejected at the highest velocities of all melt leaving the crater at this stage. This fraction would be quenched and glassy, probably impacting as hot solids. The melt ejected at lower velocities will have had less opportunity to incorporate clasts and will be deposited closer to the rim of the crater. This portion, containing a lower proportion of solids, would be hotter and thus capable of modest flow. Such a deposit would be ideal for creating the hard-rock veneer described by (Howard and Wilshire, 1975) and (Hawke and Head, 1977b). The melt remaining inside the cavity, while still probably having a notable clast content, would be the most fluid. This gradation in clast content could, therefore, account for the range of

melt occurrences around small lunar craters and could explain why small lunar craters rarely exhibit exterior melt deposits other than thin veneers.

The melt lining in the case of the complex craters, however, suffers no such disadvantages. By virtue of the greater mass of melt available for distribution along the cavity wall, even the thinner part of the melt lining near the rim will be thick enough to permit considerable ejection and sloshing over the rim in a liquid state. Much of the melt remaining in the crater, unlike the small-crater case, should also be clast free and remain molten well after the cavity has been modified. Unlike the clast-laden melt at simple craters, melt remaining on the wall after cavity growth will flow back to the bottom of the crater. Because the maximum depth of the transient cavity is attained before the maximum diameter (*e.g.*, O'Keefe and Ahrens, 1994), there will be nothing
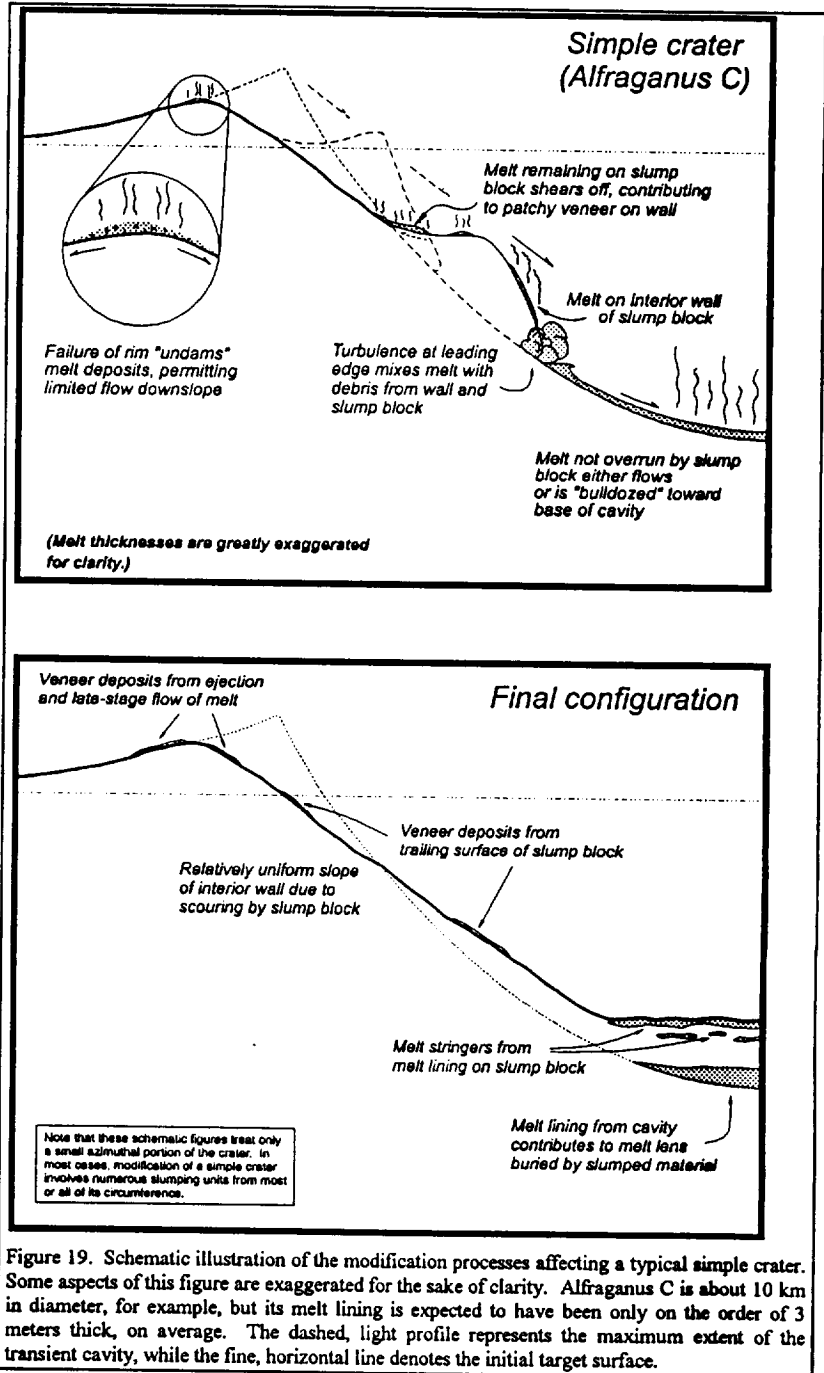
Figure 19. Schematic illustration of the modification processes affecting a typical simple crater. Some aspects of this figure are exaggerated for the sake of clarity. Alfraganus C is about 10 km in diameter, for example, but its melt lining is expected to have been only on the order of 3 meters thick, on average. The dashed, light profile represents the maximum extent of the transient cavity, while the fine, horizontal line denotes the initial target surface.

Simple crater (Alfraganus C)

Melt remaining on slump block shears off, contributing to patchy veneer on wall

Melt on interior wall of slump block

Failure of rim "undams" melt deposits, permitting limited flow downslope

Turbulence at leading edge mixes melt with debris from wall and slump block

Melt not overrun by slump block either flows or is "bulldozed" toward base of cavity

(Melt thicknesses are greatly exaggerated for clarity.)

Veneer deposits from ejection and late-stage flow of melt

Final configuration

Veneer deposits from trailing surface of slump block

Relatively uniform slope of interior wall due to scouring by slump block

Melt stringers from melt lining on slump block

Melt lining from cavity contributes to melt lens buried by slumped material

Note that these schematic figures treat only a small azimuthal portion of the crater. In most cases, modification of a simple crater involves numerous slumping units from most or all of its circumference.

preventing the central regions of the nascent complex crater from rebounding even as it is growing laterally (Grieve *et al.*, 1981; Melosh, 1989, p.142). This will further alter the flow pattern of the melt lining, as it will move downhill into the trough between the rebounding mass and the wall of the growing cavity.

The scale and style of the modification processes affecting the two crater types will be very different. Figure 19 illustrates the relatively straightforward modification of a simple crater, which occurs primarily as a consequence of slope failure of the oversteepened cavity wall (Melosh, 1989, p.128). Movement of wall material downslope (illustrated for clarity here as a mass from the rim of the crater, but more likely a more extensive movement of the entire slope) not only might smear some melt behind it as shearing at its base causes it to spread itself along the wall, but it should also "bulldoze" any melt remaining on the wall in front of it into the crater. Turbulent mixing near the leading edge of the mass should incorporate additional clastics into the melt and could also pull melt still lining the interior wall of the slump block into the mixing zone.

After the block is deposited on the crater floor, the slope will have been stabilized, as it would now possess an angle at or below the angle of repose. The remains of such blocks will compose the crater floor, with any melt remaining on its interior surface contributing to the thin veneer, or even perhaps a melt pool, on the floor. Mixing during travel downslope will be represented by stringers and pods of melt below the surface, and a melt lens, once the melt lining on and near the cavity's floor, will be buried by the debris from the wall, much as in the case of Brent (Grieve and Cintala, 1981a). In this way, the walls of simple craters are largely bereft of impact-melt deposits. Those cases in which melt pools are visible on the floor appear to occur in those structures whose walls remained at least partly in place. This would permit any melt on the wall to flow back into the crater, coalescing at the bottom to form a pool. (*e.g.*, Howard and Wilshire, 1975, Fig. 11.) The walls of such craters often display gullies and furrows that were eroded by the impact melt as it drained off the walls and onto the floor of the crater. Overall modification of simple craters is slight, with the canonical 1:5 depth/diameter ratio being somewhat lower than the 1:3 ratio assumed for the transient cavity. Such a difference can be explained easily by minor wall failure of the sort described above (Cintala, 1979; Grieve and Garvin, 1984).

The modification of larger cavities is much more complicated (Fig. 20), as it involves not only wall failure on a greater scale, but also rebound effects and voluminous melting. Perhaps most important is the difference in the shape and volume of the rebounding mass when impact melting occurs, as compared to an identical but hypothetical case in which melting does not take place. The dotted, convex-upward line on the left part of the upper pane of Fig. 20 schematically represents the shape of the rebounding mass if it were solid. As much of it is molten, however, the height and overall extent of the unmelted portion of the rebounding mass will be reduced. This differential volume will be distributed throughout the cavity and in its external deposits as melt. The lateral limit of the melt zone is represented in this interpretation as a ring of roughening around the central-peak complex (*e.g.*, Hale and Grieve, 1982). In reality, the boundary of the melt zone is almost certainly irregular (as opposed to the idealized, smooth zones represented here). The displaced blocks composing the central-peak complex would have come from a zone arranged around the point of intersection of the penetration axis and the base of the transient cavity, representing the region of deepest melting. Rebound would then cause convergence
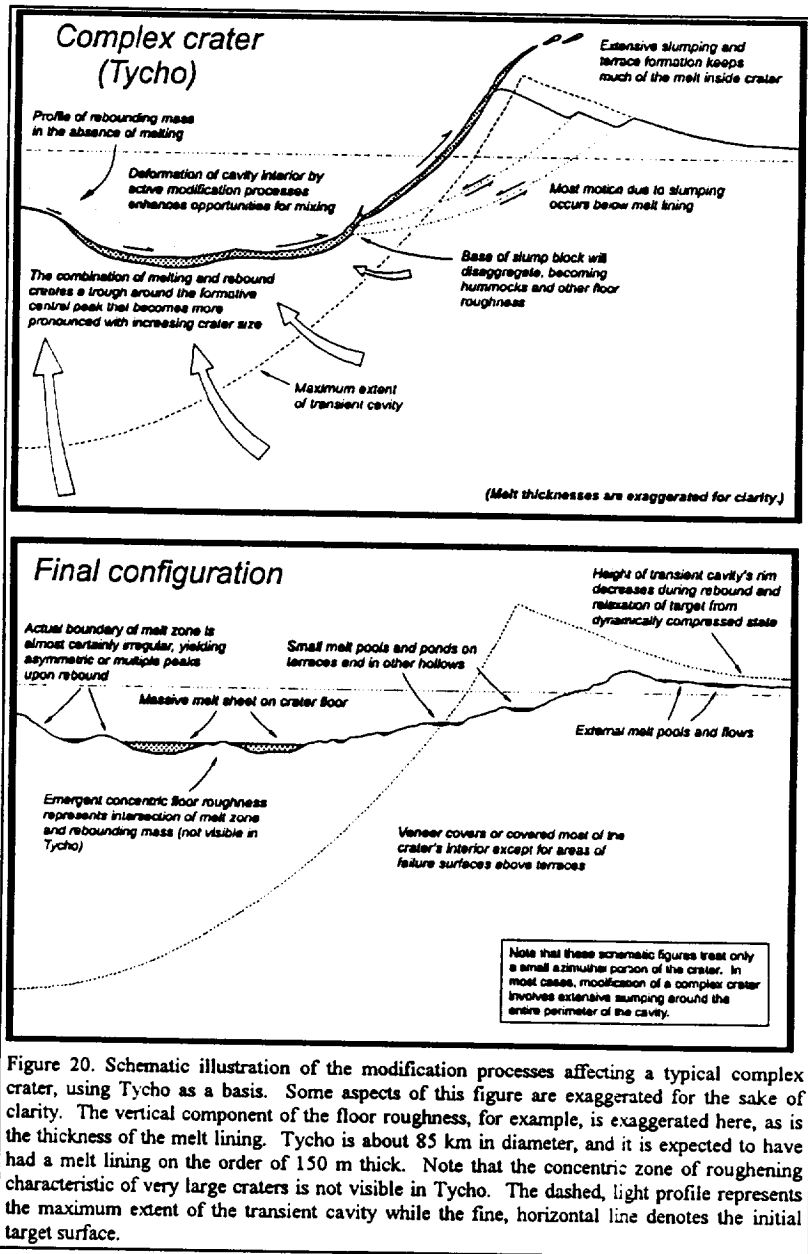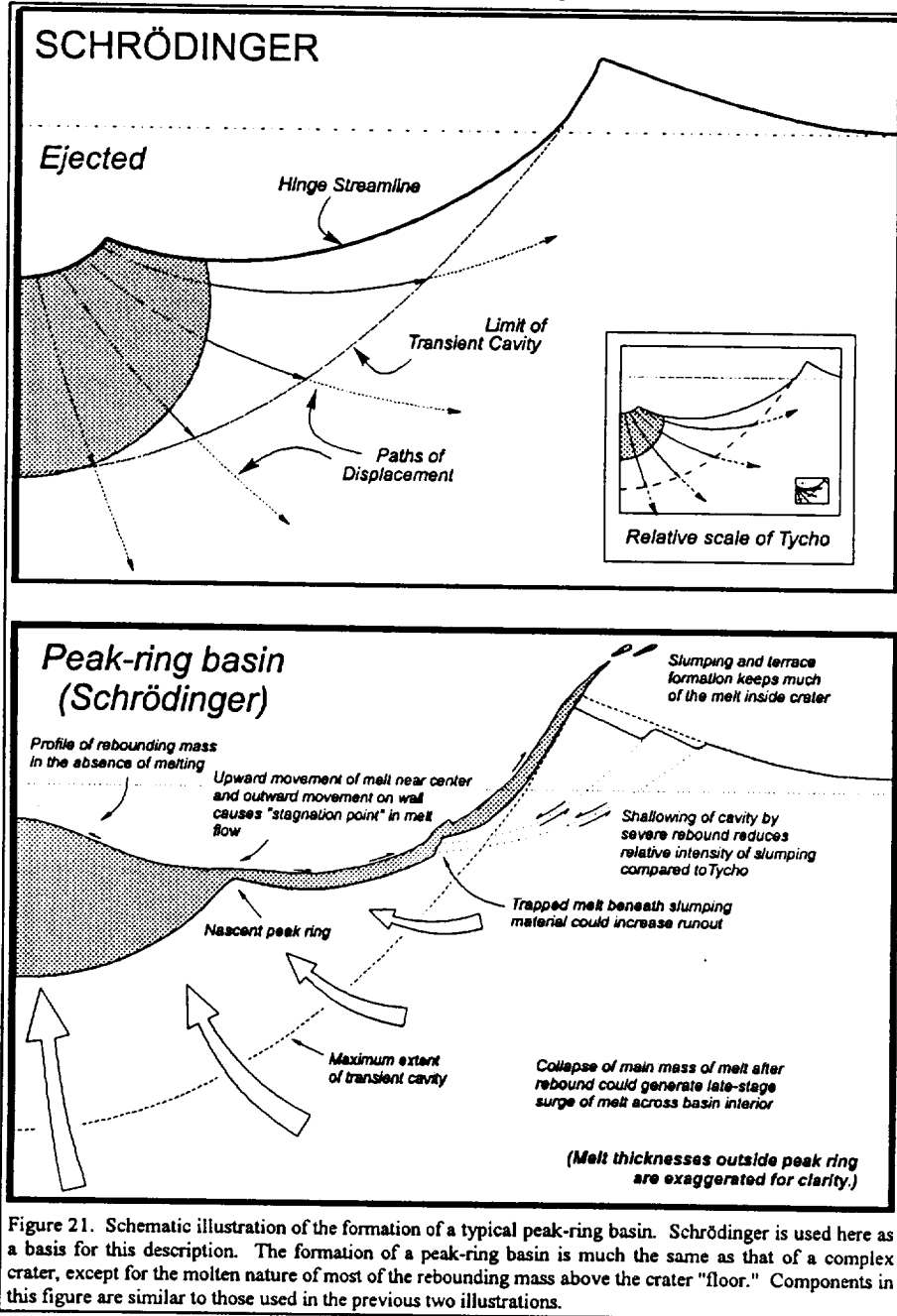

Figure 20. Schematic illustration of the modification processes affecting a typical complex crater, using Tycho as a basis. Some aspects of this figure are exaggerated for the sake of clarity. The vertical component of the floor roughness, for example, is exaggerated here, as is the thickness of the melt lining. Tycho is about 85 km in diameter, and it is expected to have had a melt lining on the order of 150 m thick. Note that the concentric zone of roughening characteristic of very large craters is not visible in Tycho. The dashed, light profile represents the maximum extent of the transient cavity while the fine, horizontal line denotes the initial target surface.

of these masses around this point, resulting in a cluster of central peaks. This suggests that the heights and volumes of these clusters of peaks in larger craters, having suffered more extensive and deeper melting, would be smaller relative to the final crater's dimensions; this is, in fact, observed (*e.g.*, Hale and Grieve, 1982), and is consistent with the hypothesis that, as larger craters are considered, impact melting is removing potential central-peak material at a greater rate than target rebound can provide it.

Wall failure in complex craters differs from that in smaller structures in that most of the shearing and displacement of the slump blocks occurs below the melt lining. In the process of moving toward the center of the crater, these blocks will disrupt any remaining upward and outward flow of the melt lining and will carry much of the melt originally on that portion of the transient cavity's rim back into the final crater. Having experienced high stress levels relative to the strength of the target rock (which is probably already fractured by previous impacts), the toes of these blocks will disaggregate as they emerge, becoming hummocks and other manifestations of floor roughness. This material, emerging from beneath and penetrating into and through the melt lining, could easily trap melt under it as it moved centripetally in the adjusting crater. This "lubrication" could aid runout of the slumping material across the crater floor.

There are, then, two manifestations of rebound in larger complex craters: the central-peak complex and the ring of roughening concentric to the peak complex. In smaller complex craters, the ring of roughening is weak enough to be buried by the melt sheet, debris from the toes of the slump blocks, or both. In the larger craters, the ring is far enough from the region of wall failure to escape the effects of burial and emerges as a feature in its own right. Antoniadi (140 km in diameter) is an example of the last vestiges of the central-peak complex remaining after the ring of roughening has emerged as the dominant central structure. Further increasing the size of the impact removes the central-peak complex entirely, thus entering the realm of peak-ring basins. To the first and perhaps even second order, the formation of peak-ring basins differs from that of complex craters only in that rebound will be more intense and the most violently rebounding mass will be predominantly impact melt.

Figure 21 schematically illustrates the main aspects of the formation of peak-ring basins under this scenario. A principal feature is the rebound of the transient cavity and the state of the rebounding materials. Centrifuge experiments described by Schmidt and Housen (1987) and cited by O'Keefe and Ahrens (1993) demonstrate that displaced target ma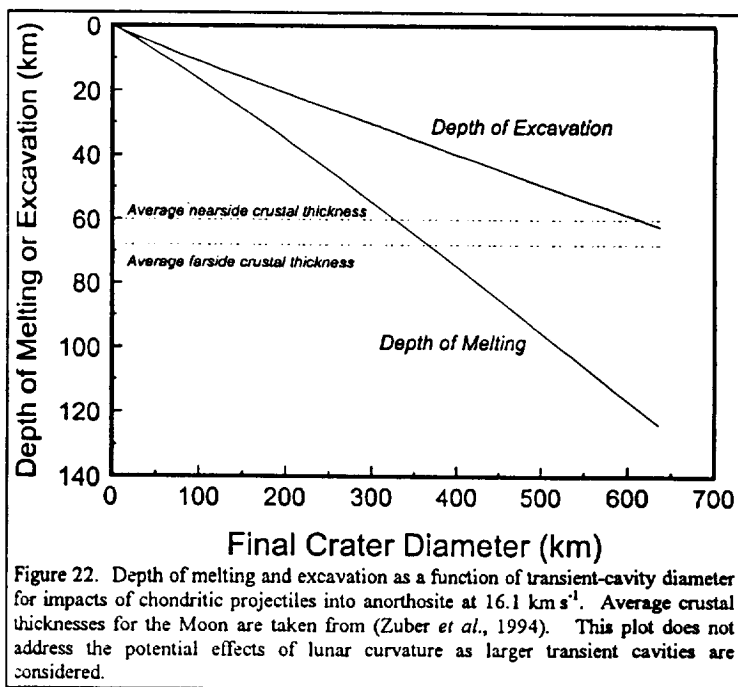terials will rebound along paths similar to the those they followed during the compression portion of the cavity's growth phase, finally stopping in the vicinity of their pre-impact positions. In this way, even though the melt lines most or all of the growing transient cavity, much of it — particularly that volume lying near the axis of rebound — will move toward the location where it was originally formed, near the center of the crater. The product of this process is another "crater" defining the limits of the melted zone, manifested ultimately as a ring, roughly concentric with the

SCHRÖDINGER

Ejected

Hinge Streamline

Limit of
Transient Cavity

Paths of
Displacement

Relative scale of Tycho

*Peak-ring basin
(Schrödinger)*

Profile of rebounding mass
in the absence of melting

Upward movement of melt near center
and outward movement on wall
causes "stagnation point" in melt
flow

Slumping and terrace
formation keeps much
of the melt inside crater

Shallowing of cavity by
severe rebound reduces
relative intensity of slumping
compared to Tycho

Trapped melt beneath slumping
material could increase runout

Nascent peak ring

Maximum extent
of transient cavity

Collapse of main mass of melt after
rebound could generate late-stage
surge of melt across basin interior

(Melt thicknesses outside peak ring
are exaggerated for clarity.)

Figure 21. Schematic illustration of the formation of a typical peak-ring basin. Schrödinger is used here as a basis for this description. The formation of a peak-ring basin is much the same as that of a complex crater, except for the molten nature of most of the rebounding mass above the crater "floor." Components in this figure are similar to those used in the previous two illustrations.

basin's rim crest (Fig. 21). The shape of this ring would change with increasing obliquity of impact, reflecting the geometry of the peak-stress contours and possibly explaining the more elliptical rings, such as that found in Antoniadi.

Because rebound is well underway before lateral growth of the cavity has ceased, the relative depth of the cavity would, at any given time during its modification, be reduced relative to that of a crater the size of Tycho, for instance. With a correspondingly smaller relative difference in height between the "rim crest" and the foot of the "wall," the relative magnitude of wall failure should be less severe than in a complex, but deeper, crater. On the other hand, the centripetal accelerations that characterize the rebound process should undermine the walls of the cavity, enhancing the conditions for wall failure. It is because of these potential complicating factors that we apply Croft's (1985) modification-scaling relationship to the peak-ring basins with some hesitation. It should be emphasized that this picture of wall failure does not conflict with the "megaterrace" hypothesis of (Head, 1974a), as that mechanism occurs on an even greater scale than that described here.

The relative depths of melting and excavation become important in large events (*e.g.*, Tonks and Melosh, 1993). Figure 22 shows the trends for impacts at 16.1 km s^{-1}, along with the average crustal thicknesses as determined by (Zuber *et al.*, 1994). Only transient-cavity diameters are plotted in this figure, since the largest events represented in this graph approach the scale of multiring basins (*e.g.*, Spudis, 1993). As indicated above, the modification processes involved at those scales are poorly understood at best. An additional factor not addressed here is the potential effect of lunar curvature on both the excavation and modification phases of these structures. Clearly, the larger the structure, the more likely it is that

Figure 22. Depth of melting and excavation as a function of transient-cavity diameter for impacts of chondritic projectiles into anorthosite at 16.1 km s^{-1}. Average crustal thicknesses for the Moon are taken from (Zuber *et al.*, 1994). This plot does not address the potential effects of lunar curvature as larger transient cavities are considered.

curvature effects will come into play (*e.g.*, Tonks and Melosh, 1993).

The depth of melting overtakes the depth of excavation very quickly with increasing cavity size, and the two trends diverge rapidly as a function of cavity diameter. Melting would be confined to the crust until transient-cavity diameters of about 200 and 240 km for the average nearside and farside, respectively. When excavation exceeds pass the base of the crust, melting will occur at more than twice that depth on either side. It is difficult to imagine how the large impact basins such as Imbrium and Orientale could not have melted to depths well below the crust, even though their limits of excavation could have been confined to the crust (Ryder *et al.*, 1997). Thus, the massive, coherent impact-melt deposits associated with large lunar basins could possess compositions different from their ejecta, as deep crustal and mantle materials would constitute a greater component of these melts (Warren *et al.*, 1996). With suitable topography to hold the vast volumes created during such events, melt bodies kilometers thick could be trapped; the extended times taken to cool these deposits could then lead to differentiation processes (Grieve *et al.*, 1991; Spudis, 1993) and hence to petrologic types that might not be expected otherwise.

Finally, as a corollary of the model, peak rings will originate at shallower depths than the maximum depth of impact melting. Thus, the most deeply exposed solid materials within the basin — the ring itself — will be derived from stratigraphic levels located above the depth of origin of much of the impact melt composing the basin's floor. This could explain the observations that some peak rings appear to be anorthositic in composition (*e.g.*, Spudis *et al.*, 1984; Hawke *et al.*, 1995).
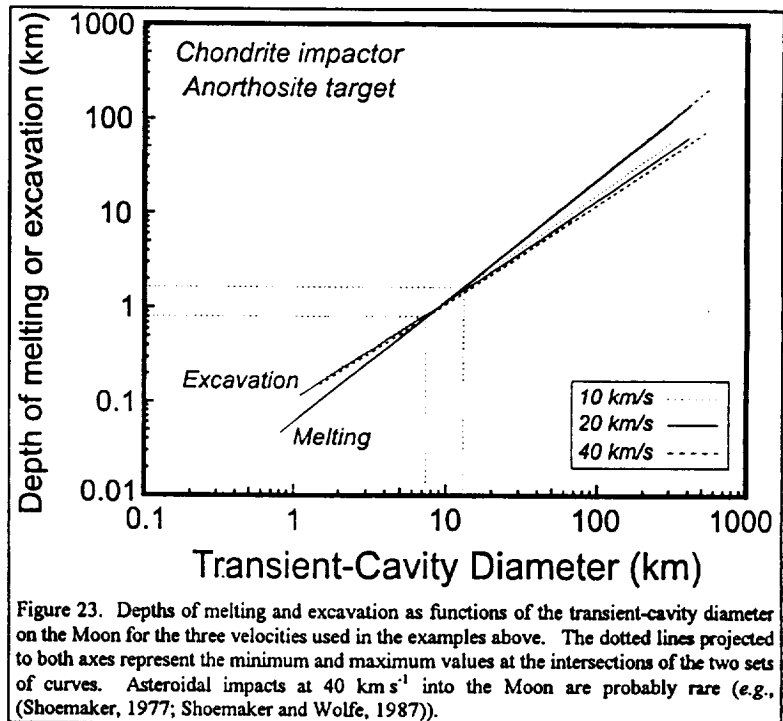
Depth of Melting vs. Depth of Excavation

The provenance of lunar-samples and interpretation of remote-sensing data usually depend on some knowledge of the depth of origin of the materials in question. Due to the uncertainties involved in modeling the volumes and paths of excavation for large craters with the precision desired for the interpretation of samples, however, such information is generally unavailable. Along with the excavation, ejection, and ejecta emplacement, impact melting is another means of deriving material from depth and depositing it at the surface. Little attention, however, has been given to impact melting as a means of deep sampling because it leaves a highly complicated imprint on the sample. Nevertheless, the deepest materials exposed

at the surface of the Moon are probably the products of impact melting. It might be thought that central structures consistently represent the deepest materials exposed by impact, but it will be shown below that this probably is not the case.

The maximum depth of excavation in any given velocity field specified by the z-model can be determined by the inflection point on the hinge streamline in a cartesian coordinate system (see, for example, Croft, 1980). The values thus determined are plotted as a function of transient-cavity diameter in Fig. 23, along with curves for the maximum depth of melting. This plot shows that, given the model constraints used here, melting has the potential of bringing to the surface deeper material than excavation during the formation of transient cavities larger than 8.5 to 13 km in diameter. Conversely, if a sample were identified as having been derived from a depth greater than, say, 1.5 km, it is likely that deeper material would have been brought to the surface as a component of that crater's impact-melt deposits. It is important to remember, however, that such originally deep-seated material will be a variable component of the resulting impact-melt deposits, which will have sampled the total relevant stratigraphy (Dence *et al.*, 1976; Kring, 1997). In addition, as such melt deposits cool, their component mineralogy will reflect their averaging

Figure 23. Depths of melting and excavation as functions of the transient-cavity diameter on the Moon for the three velocities used in the examples above. The dotted lines projected to both axes represent the minimum and maximum values at the intersections of the two sets of curves. Asteroidal impacts at 40 km s⁻¹ into the Moon are probably rare (*e.g.*, (Shoemaker, 1977; Shoemaker and Wolfe, 1987)).

nature and the surface crystallization environment; that is, although the impact melt from a large impact event might have sampled deeper material than the associated ejecta, the deep source might not be readily apparent in data obtained by remote-sensing instrumentation (Pieters *et al.*, 1997).

If only highly oblique impacts were plotted, this figure would change; see, for example, the schematic diagrams of (O'Keefe and Ahrens, 1986) of energy and momentum transfer to the target during highly oblique impact.

Impact Melting, Stratigraphic Uplift, and the Depths of Origin of Central Peaks

The zone of melting in sufficiently large impacts overlaps the region in the target that spawns central structures. Since melt cannot participate in the construction of central peaks except in trace amounts (*e.g.*, as injected material in dikes, veneer on the exterior of the peak, *etc.*), impact melting removes material from the peak-formation process as efficiently as ejection. Consequently, the minimum depth of origin of central peaks for vertical to near-vertical impacts can be established by examining the maximum depth of melting for the crater-producing event (Cintala and Grieve, 1992; Fig. 24). Central peaks on the Moon begin to appear at crater diameters near 10 km and persist to diameters as large as 200 km (Tsiolkovsky). The central peak in such a crater could have originated as deep as 35 km, still within the crust (Zuber *et al.*, 1994). This relationship between depth of melting and the origin of central peaks

was used by (Cintala and Grieve, 1994) to estimate the amount of stratigraphic uplift represented by lunar central peaks. The results presented in that paper, however, contain a scaling error that had the unfortunate effect of exaggerating the difference between the Earth and the Moon for this phenomenon. The data and calculations are presented here in their correct form; they and the following interpretations supersede those in (Cintala and Grieve, 1994).
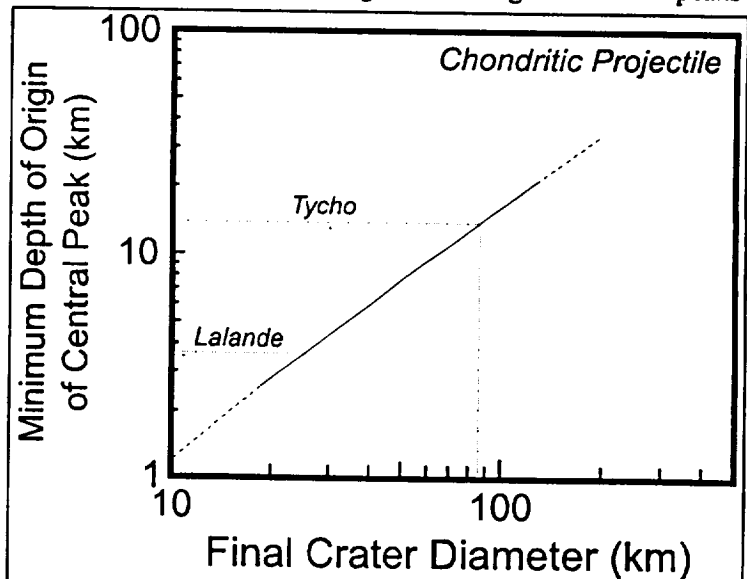

Figure 24. Minimum depth of origin of central-peak material as a function of final crater diameter for lunar impacts. This curve represents impacts at 16.1 km s⁻¹, but curves generated at other reasonable velocities would be almost indistinguishable from this one at this scale. The diameter to which central peaks persist is not established (Spudis, 1993) and their appearance as a function of size is a gradual one, hence the dashed ends of the curve.

The magnitude of stratigraphic uplift u_s can be related to the depth of melting d_m and the depth from the original target surface to the top of the peak d_p (Fig. 25) through

$$u_s = d_m - d_p \tag{11}$$

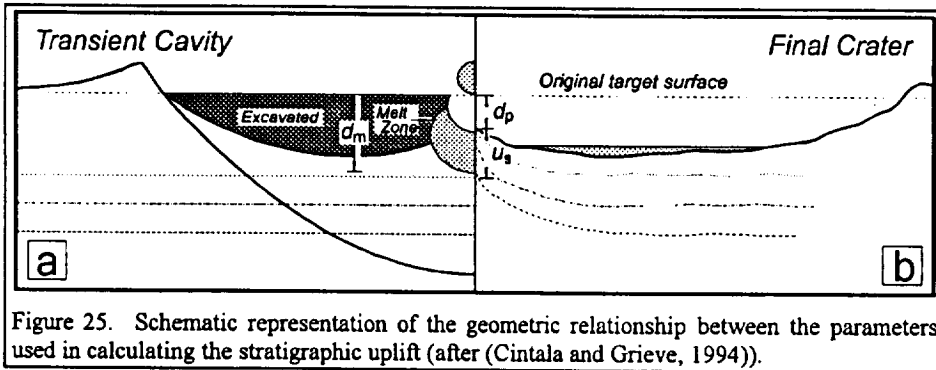Topographic data exist at sufficient resolution for a number of large, fresh lunar craters, but only those in the maria can be used in this case, as the exterior topography in more rugged highland terrain does not permit accurate measurement of d_p. Measurements were

Figure 25. Schematic representation of the geometric relationship between the parameters used in calculating the stratigraphic uplift (after (Cintala and Grieve, 1994)).

made on twelve such craters, with the results given in Table 4.

Some large craters, such as Tsiolkovsky, possess single central peaks, indicating that the boundary of the melt zone was better defined and more symmetrical than in craters with clusters of peaks. In such cases of single peaks, the maximum depth of melting can be used to fix the minimum depth of origin of the main central peak. Multiple peaks, however, typically occur as a group of satellite hills or large hummocks around or near the main peak. These smaller peaks probably originate at shallower locations off the penetration axis, brought
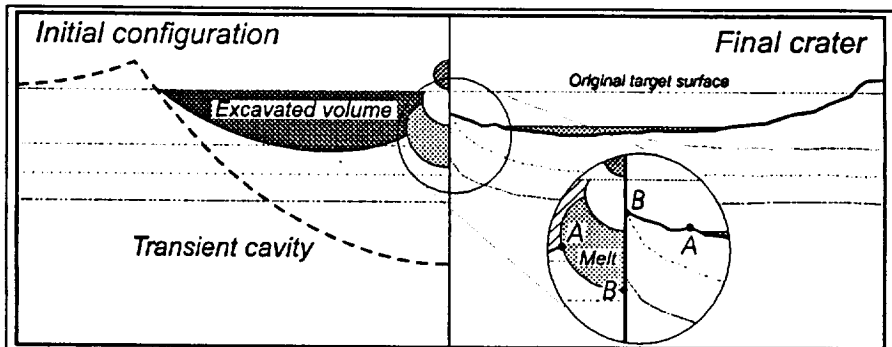

Figure 26. Schematic diagram illustrating a possible geometry explaining the formation of multiple central peaks. The points A and B on the left of the inset correspond to their counterparts on the right. Because A lies at a shallower initial depth than that of B, only the minimum depth of origin of the main peak can be estimated by the maximum depth of melting. This geometry implies that satellite peaks originate off the axis of melting.

toward the center of the crater during centripetal collapse of the transient cavity (Fig. 26).

Table 4. Morphometric parameters for the lunar craters used in estimating stratigraphic uplift. Most of the values for D_r and d_p were taken from (Hale and Grieve, 1982). Values for D_{tc} and u_s were determined as described in the text.

Crater	D_r (km)	D_{tc} (km)	d_p (km)	u_s (km)
Dawes	17.0	17.0	1.4	1.0
Pierce	18.5	18.5	1.1	1.6
Picard	23.2	22.5	1.4	2.2
Delisle	25.0	23.9	1.3	2.6
Mädler	27.5	26.0	1.6	2.7
Lambert	30.0	28.0	1.3	3.4
Kant	31.0	28.7	2.4	2.5
Timocharis	33.0	30.3	1.4	3.8
Plinius	41.0	36.4	0.7	5.9
Shirakatsi	46.2	40.3	1.5	6.0
Brunner	51.5	44.2	0.8	7.6
Langrenus	136	101	1.1	23.3

As was done in (Cintala and Grieve, 1994), the points for the lunar craters are plotted in Fig.27 along with values estimated for a group of terrestrial craters for comparison [Grieve, 1996 #496; Table 5]. Log-log least-squares fits to the two data sets give

$$u_s = 0.022 D_r^{1.45} \tag{12}$$

for the lunar case ($r = 0.983$) and

$$u_s = 0.086 D_r^{1.03} \tag{13}$$

for the terrestrial data ($r = 0.979$). A t-test comparing the slopes of these fits indicates that, at a confidence level above 99.95%, these data are not from the same population. Having noted the results of the statistical test, too much should not be made of these differences. It can be stated with some confidence that this disparity is not due to post-excavation enlargement of the crater through the modification mechanisms treated by (Croft, 1985), because the difference in slope persists when the derived transient-cavity diameter is used instead as the independent variable (Fig. 28).

The terrestrial sample used in these comparisons contains craters that have been eroded to varying degrees, certainly more severely than the lunar group. The lunar values were derived by calculating the minimum possible depth of origin of the central peaks. Should some process remove material from the peak subsequent to the melting

Table 5. Data from (Grieve and Pilkington, 1996) for terrestrial craters whose values of stratigraphic uplift have been estimated. These values were taken from various sources in the published literature, which accounts for the variations in significant figures.

| Crater	D_r(km)	D_{tc} (km)	u_s (km)
Glasford	4	4.0	0.3
Il'inets	4.5	4.4	0.3
Steinheim	3.8	3.8	0.4
Flynn Creek	3.8	3.8	0.4
Tin Bider	6	5.7	0.5
Decaturville	6	5.7	0.5
Upheaval Dome	10	8.8	0.6
Wells Creek	12	10.2	0.7
Red Wing	9	8.0	0.9
Rogozinskaya	9	8.0	1.0
Marquez	12.7	10.7	1.1
Sierra Madera	13	10.9	1.2
Eagle Butte	10	8.8	1.3
Steen River	25	19.1	1.7
Lawn Hill	18	14.4	2.0
Haughton	24	18.4	2.0
Teague	30	22.3	2.5
Longancha	20	15.8	2.7
Gosses Bluff	22	17.1	3.0
Manson	35	25.4	3.5
Siljan	52	35.5	4.6
Kara	65	43.0	5.5
Charlevoix	54	36.7	6.0
Vredefort	300	158	30
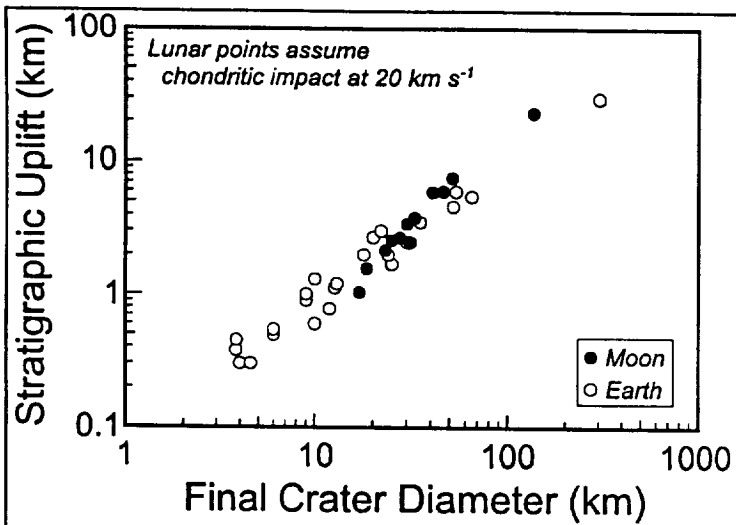
Figure 27. Amount of stratigraphic uplift as a function of final crater diameter calculated for lunar craters. Data points for terrestrial craters represent values presented in (Grieve and Pilkington, 1996) and Table 5. While the spatial agreement in this plot is good, the data for the two planets come from statistically distinct populations.

stage of the event — such as slumping of material from the summit and sides during the rebound stage of central-uplift formation — then the stratigraphic uplift for the lunar craters could be even greater. Such a process could also be size-dependent, further complicating a detailed comparison. As a result, the comparison between the two planets is ambiguous, and must await better data, a new method of estimating the amount of stratigraphic uplift, or a means of reconstructing terrestrial craters with much greater accuracy than is currently available.

SUMMARY REMARKS

The process of differential scaling is the result of melt production growing faster than crater size as impact magnitude increases. By combining a model of impact-melt generation and Maxwell's z-model to approximate crater growth and ejection geometries, a variety of implications for the role of impact melting in the nature of lunar craters can be inferred.
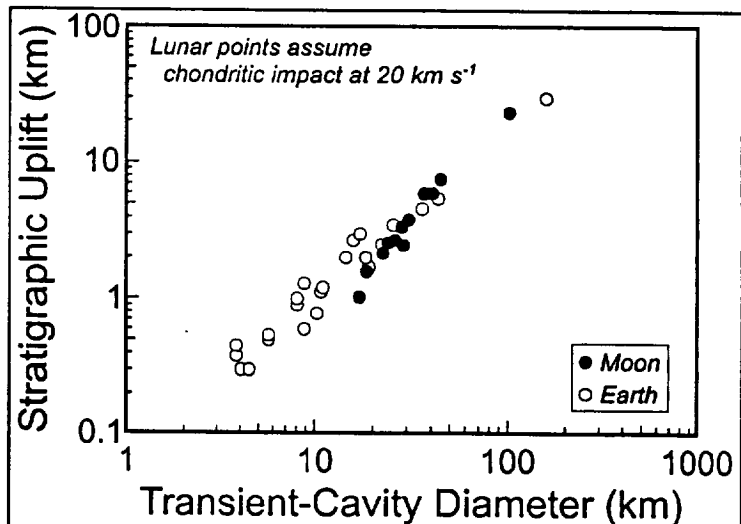

Figure 28. Amount of stratigraphic uplift as a function of transient-cavity diameter calculated for lunar craters. Data points for terrestrial craters represent values presented in (Grieve and Pilkington, 1996) and Table 5. Variations in the assumed impact velocity in the lunar calculations would make no noticeable difference in this plot.

Lunar simple craters suffer limited effects from impact melting; indeed, the relative volumes of melt are so small that the resulting deposits give only moderate indication of having been liquid. This is

due primarily to the chilling effects of clast incorporation into the thin melt lining of the transient cavity during its growth. The depth of ejection for lunar simple craters appears to be consistently deeper than the maximum depth of melting. The transition in morphology from simple to complex craters occurs in the same diameter range at which the depth of melting overtakes that of ejection. Whether a causal relationship exists between these two transitions is unknown, but it might be more than coincidental. Rebound in simple craters is negligible, and thus no information regarding the extent of the zone of melting is preserved in such structures.

Transitional lunar craters — those between simple and complex structures — begin to display signs of impact melting that are easily observable in orbital photography. Pools, ponds, sheets, and flows of impact melt occur in most fresh craters between about 15 and 30 km in diameter. Small central peaks and the beginnings of terraced walls also make an appearance in these craters. The depth of melting exceeds that of ejection in these impacts, and the relative volume of clastics incorporated into the impact melt as a whole is less than in the case of the simple craters. The depth of origin of the main central peak in such craters may reflect the depth of melting.

Complex lunar craters, which include those with well-developed wall terraces and central-peak complexes, are greatly affected by impact melting. Not only is evidence for impact melt everywhere on the interior and the immediate exterior environs of such craters, but impact melting plays a role in the formation and interior morphology of the structures themselves. The volume of melt is sufficient to alter the interior morphometry of the structure, and a major fraction of the clastic material incorporated into the melt mass is digested by the superheated liquid. Extensive impact melting occurs at depths well below that of ejection. Multiple central peaks probably originate in a zone surrounding the maximum depth of melting, and thus can be used only to fix the minimum depth of melting; conversely, the maximum depth of melting can be treated as the minimum possible depth of origin of central peaks in these craters. Impact melting decreases the volume of the central peaks in these large structures relative to that expected from simple extrapolation of the peak-volume vs. crater-size relationship that describes smaller craters. While the total volume of rebounding material might be predicted by such an extrapolation, much of that volume is molten in the case of the larger craters and thus cannot be part of the topographic expression of that

rebound. The "ring of roughening" observed in very large central-peak craters is interpreted here as the signature of the lateral extent of the rebounded melt zone.

Peak-ring basins are a consequence of the differential scaling hypothesis, with the rings being "mature" rings of roughening seen in the large central-peak craters. Melting in a peak-ring basin extends to depths much greater than that of ejection, and to depths well below the depth of origin of the ring itself. The proportion of clasts incorporated into such melt volumes is insignificant from a bulk-chemical point of view, and clasts are not a major factor in controlling the viscosity and thermal history of melts in such structures. Indeed, the volume of melt trapped within a peak-ring basin should be able to evolve into a differentiated unit as it cools.

The limited nature of the models used in this study preclude the ability to examine the detailed motions of the target during the formation of lunar craters and basins. While we believe that the relative relationships as stated are realistic, they cannot be used as absolute guidelines. Barring extensive field work at such structures, only much more detailed model calculations and remote-sensing information can test the suggestions made here.

ACKNOWLEDGEMENTS

REFERENCES

Ahrens T.J. and O'Keefe J.D. (1972) Shock melting and vaporization of lunar rocks and minerals. *The Moon* 4, 59-94.

Austin M.G., Thomsen J.M., Ruhl S.F., Orphal D.L. and Schultz P. H. (1980) Calculational investigation of impact cratering dynamics: Material motions during the crater growth period. *Proc. Lunar Planet. Sci. Conf. 11th*, 2325-2345.

Chabai A.J. (1965) On scaling dimensions of craters produced by buried explosives. *J. Geophys. Res.* 70, 5075-5098.

Chabai A.J. (1977) Influence of gravitational fields and atmospheric pressures on scaling of explosion craters. In *Impact and Explosion Cratering* (eds. D.J. Roddy, R.O. Pepin and R.B. Merrill), pp. 1191-1214. Pergamon Press, New York, NY.

Cintala M.J. (1979) Mercurian crater rim heights and some interplanetary comparisons. *Proc. Lunar Planet. Sci. Conf. 10th*, 2635-2650.

Cintala M.J. (1992) Impact-induced thermal effects in the lunar and mercurian regoliths. *J. Geophys. Res.* 97, 947-974.

Cintala M.J. and Grieve R.A.F. (1984) Energy partitioning during terrestrial impact events: Melt production and scaling laws (abstract). *Lunar Planet Sci. XV*, 156-157.

Cintala M.J. and Grieve R.A.F. (1991) Impact melting and peak-ring basins: Interplanetary considerations (abstract). *Lunar Planet Sci. XXII*, 215-216.

Cintala M.J. and Grieve R.A.F. (1992) Melt production in large-scale impact events: Calculations of impact-melt volumes and crater scaling (abstract). In *Papers Presented to the International Conference on Large Meteorite Impacts and Planetary Evolution*, pp. 13-14. Lunar and Planetary Institute, Houston, TX.

Cintala M.J. and Grieve R.A.F. (1994) The effects of differential scaling of impact melt and crater dimensions on lunar and terrestrial craters: Some brief examples. In *Large Meteorite Impacts and Planetary Evolution* (eds. Burkhard O. Dressler, R.A.F. Grieve and V. L. Sharpton), pp. 51-59. Geological Society of America, Boulder, CO.

Cintala M.J., Wood C.A. and Head J.W. (1977) The effects of target characteristics on fresh crater morphology: Preliminary results for the Moon and Mercury. *Proc. Lunar Planet. Sci. Conf. 8th*, 3409-3425.

Croft S.K. (1977) Energies of formation for ejecta blankets of giant impacts. In *Impact and Explosion Cratering* (eds. D. J. Roddy, R. O. Pepin and R. B. Merrill), pp. 1279-1296. Pergamon Press, New York.

Croft S.K. (1980) Cratering flow fields: Implications for the excavation and transient expansion stage of crater formation. *Proc. Lunar Planet. Sci. Conf. 11th*, 2347-2378.

Croft S.K. (1981a) The excavationstage of basin formation: A qualitative model. In *Multi-Ring Basins* (eds. P.H. Schultz and R.B. Merrill), pp. 207-225. Pergamon, New York.

Croft S.K. (1981b) The modification stage of basin formation: Conditions of ring formation. In *Multi-Ring Basins* (eds. P.H. Schultz and R.B. Merrill), pp. 227-257. Pergamon, New York.

Croft S.K. (1983) A proposed origin for palimpsests and anomalous pit craters on Ganymede and Callisto. In *Proc. Lunar Planet Sci. Conf. 14th*, in *J. Geophys. Res.* **88**, B71-B89.

Croft S.K. (1985) The scaling of complex craters. *Proc. Lunar Planet Sci. Conf. 15th* **89**, in *J. Geophys. Res.*, C828-C842.

Dence M.R. (1971) Impact melts. *J. Geophys. Res.* **76**, 5552-5565.

Dence M.R. (1973) Dimensional analysis of impact structures. *Meteoritics* **8**, 343-344.

Dence M.R., Grieve R.A.F. and Plant A.G. (1976) Apollo 17 grey breccias and crustal composition in the Serenitatis Basin region. *Proc Lunar Sci. Conf. 7th*, 1821-1832.

Duvall G.E. (1958) Pressure-volume relations in solids. *AM.J. Physics.* **26**, 235-238.

Floran R.J., Grieve R.A.F., Phinney W.C., Warner J.L., Simonds C.H., Blanchard D.P. and Dence M.R. (1978) Manicouagan impact melt, Quebec, 1. Stratigraphy, petrology, and chemistry. *J. Geophys. Res.* **83**, 2737-2759.

French B.M. and Short N.M. (1968) *Shock Metamorphism of Natural Materials*, Mono Book Corporation, Baltimore. 644 pp.

Gault D.E. and Heitowit E.D. (1963) The partition of energy for hypervelocity impact craters formed in rock. *Proc. Hypervel. Impact Sympos. 6th*, 419-456.

Grieve R.A.F. (1980) Cratering in the lunar highlands: Some problems with the process, record and effects. In *Proceedings of the Conference on the Lunar Highlands Crust* (eds. J. J. Papike and R. B. Merrell), pp. 173-196. Pergamon Press, New York.

Grieve R.A.F. (1988) The Haughton impact structure: Summary and synthesis of the results of the HISS project. *Meteoritics* **23**, 249-254.

Grieve R.A.F. and Cintala M.J. (1981a) Brent Crater, Ontario: Observation and theory (abstract). *Lunar Planet. Sci. XII*, 362-364.

Grieve R.A.F. and Cintala M.J. (1981b) A method for estimating the initial impact conditions of terrestrial cratering events, exemplified by its application to Brent Crater, Ontario. *Proc. Lunar Planet. Sci. Conf. 12th*, 1607-1621.

Grieve R.A.F. and Cintala M.J. (1991) Differential scaling of crater parameters: Implications for the observed terrestrial record (abstract). *Lunar Planet. Sci. XXII*, 493-494.

Grieve R.A.F. and Cintala M.J. (1992a) An analysis of differential impact melt-crater scaling and implications for the terrestrial impact record. *Meteoritics* **27**, 526-538.

Grieve R.A.F. and Cintala M.J. (1992b) Melt production in large-scale impact events: Implications and observations at terrestrial craters (abstract). In *Papers Presented to the International Conference on Large Meteorite Impacts and Planetary Evolution*, pp. 32-33. Lunar and Planetary Institute, Houston, TX.

Grieve R.A.F. and Cintala M.J. (1997) The early Earth: No large lunar-like multiring impact basins. submitted to *Nature*.

Grieve R.A.F., Dence M.R. and Robertson P.B. (1977) Cratering Process: As interpreted from the occurrence of impact melts. In *Impact and Explosion Cratering* (eds. D.J. Roddy, R.O. Pepin and R. B. Merrill), pp. 791-814. Pergamon Press, New York.

Grieve R.A.F. and Floran R.J. (1978) Manicouagan impact melt, Quebec, 2. Chemical interrelations with basement and formational process. *J. Geophys. Res.* 83, 2761-2771.

Grieve R.A.F. and Garvin J.B. (1984) A geometric model for excavation and modification at terrestrial simple impact craters. *J. Geophys. Res.* 89, 11561-11572.

Grieve R.A.F., Garvin J.B., Coderre J.M. and Rupert J. (1989) Test of a geometric model for the modification stage of simple impact crater development. *Meteoritics* 24, 83-88.

Grieve R.A.F. and Pesonen L.J. (1992) The terrestrial impact cratering record. *Tectonophysics* 216, 1-30.

Grieve R.A.F. and Pilkington M. (1996) The signature of terrestrial impacts. *AGSO Jour. Australian Geol. Geophys.* 16, 399-420.

Grieve R.A.F., Plant A.G. and Dence M.R. (1974) Lunar impact melts and terrestrial analogs: Their characteristics, formation and implications for lunar crustal evolution. *Proc. Lunar Sci. Conf. 5th*, 261-273.

Grieve R.A.F. and Robertson P.B. (1979) The terrestrial cratering record: I. Current status of the observations. *Icarus* 38, 212-229.

Grieve R.A.F., Robertson P.B. and Dence M.R. (1981) Constraints on the formation of ring impact structures, based on terrestrial data. In *Multi-Ring Basins, Proc. Lunar Planet. Sci Conf. 12A*, 37-57.

Grieve R.A.F., Stöffler D. and Deutsch A. (1991) The Sudbury Structure: Controversial or misunderstood? *J. Geophys. Res.* 96, 2753-22764.

Hale W.S. and Grieve R.A.F. (1982) Volumetric analysis of complex lunar craters: Implications for basin ring formation. *Proc. Lunar Planet. Sci. Conf. 13th*, in *Jour. Geophys. Res.* 87, A65-A76.

Hale W.S. and Head J.W. (1979) Central peaks in lunar craters: Morphology and morphometry. *Proc. Lunar Planet. Sci. Conf. 10th*, 2623-2633.

Hawke B.R. and Head J.W., III (1977a) Impact melt in lunar crater interiors (abstract). *Lunar Sci. VIII*, 415-417.

Hawke B.R. and Head J.W., III (1977b) Impact melt on lunar crater rims. In *Impact and Explosion Cratering* (eds. D.J. Roddy, R.O. Pepin and R.B. Merrill), pp. 815-841. Pergamon, New York.

Hawke B.R., Peterson C.A., Lucey P.G., Taylor G.J., Blewett D.T. and Spudis P.D. (1995) Remote sensing studies of lunar anorthosite deposits (abstract). *Lunar Planet. Sci. XXVI*, 563-564.

Head J.W., III (1974a) Orientale multi-ringed basin interior and implications for the petrogenesis of lunar highland samples. *The Moon* 11, 327-356.

Head J.W., III (1974b) Stratigraphy of the Descartes Region (Apollo 16): Implications for the Origin of Samples. *The Moon* 11, 77-99.

Head J.W., III (1976) The significance of substrate characteristics in determining morphology and morphometry of lunar craters. *Proc. Lunar Sci. Conf 7th*, 2913-2929.

Holsapple K.A. and Schmidt R.M. (1980) On the scaling of crater dimensions 1. Explosive processes. *J. Geophys. Res.* 85, 7247-7256.

Holsapple K.A. and Schmidt R.M. (1982) On the scaling of crater dimensions 2. Impact processes. *J. Geophys. Res.* 87, 1849-1870.

Holsapple K.A. and Schmidt R.M. (1987) Point source solutions and coupling parameters in cratering mechanics. *J. Geophys. Res.* 92, 6350-6376.

Hörz F., Ostertag R. and Rainey D.A. (1983) Bunte Breccia of the Ries: Continuous deposits of large impact craters. *Rev. Geophys. Space Phys.* 21, 1667-1725.

Howard K.A. (1974) Fresh lunar impact craters: Review of variations with size. *Proc. Lunar Sci. Conf. 5th*, 61-69.

Howard K.A. and Wilshire H.G. (1975) Flows of impact melt in lunar craters. *Journal of Research of the U.S. Geological Survey* 3, 237-251.

Ivanov B.A. (1988) Effect of modification of impact craters on the size-frequency distribution and scaling law (abstract). *Lunar Planet. Sci. XIX*, 531-532.

Kieffer S.W. and Simonds C.H. (1980) The role of volatiles and lithology in the impact cratering process. *Rev. Geophys. Space Phys.* 18, 143-181.

Kring D.A. (1997) Composition of Earth's continental crust as inferred from the compositions of impact melt sheets (abstract). *Lunar Planet. Sci. XXVIII*, 763-764.

Mackin J.H. (1969) Origin of lunar maria. *Geol. Soc. Amer. Bull.* 80, 735-748.

Maxwell D.E. (1973) Cratering flow and crater prediction methods. Physics International Co.

Maxwell D.E. (1977) Simple Z model of cratering, ejection, and the overturned flap. In *Impact and Explosion Cratering* (eds. D.J. Roddy, R.O. Pepin and R.B. Merrill), pp. 1003-1008. Pergamon, New York.

McCauley J.F. (1977) Orientale and Caloris. *Phys.Earth .Planet. Inter.* 15, 220-250.

McKay D.S., Greenwood W.R. and Morrison D.A. (1970) Origin of small lunar particles and breccia from the Apollo 11 site. *Proc. Apollo 11 Lunar Sci. Conf.*, 673-694.

McKinley J.P., Taylor G.J., Keil K., Ma M.-S. and Schmitt R.A. (1984) Apollo 16: Impact melt sheets, contrasting nature of the Cayley Plains and Descartes Mountains, and geologic history. In *Proc. Lunar Planet. Sci. Conf. 14th*, in *J. Geophys. Res.* 88, B513-B524.

McQueen R.G., Marsh S.P. and Fritz J.N. (1967) Hugoniot equation of state of twelve rocks. *J. Geophys. Res.* 72, 4999-5036.

Melosh H.J. (1989) *Impact Cratering -- A Geologic Process*. Oxford, New York. 245pp..

Moore H.J., Hodges C.A. and Scott D.H. (1974) Multiringed basins -- illustrated by Orientale and associated features. *Proc. Lunar Sci. Conf. 5th*, 71-100.

Naldrett A.J. and Hewins R.N. (1984) The main mass of the Sudbury Igneous Complex. In *The Geology and Ore Deposits of the Sudbury Structure* (eds. E.G. Pye, A.J. Naldrett and P.E. Giblin), pp. 235-251. Ministry of Natural Resources, Toronto, Ontario.

Oberbeck V.R. and Quaide W.L. (1967) Estimated thickness of a fragmental surface layer of Oceanus ProcellaruM.J. *Geophys. Res.* 72, 4697-4704.

O'Keefe J.D. and Ahrens T.J. (1977) Impact-induced energy partitioning, melting, and vaporization on terrestrial planets. *Proc. Lunar Sci. Conf. 8th*, 3357-3374.

O'Keefe J.D. and Ahrens T.J. (1986) Oblique impact: A process for obtaining meteorite samples from other planets. *Science* 234, 346-349.

O'Keefe J.D. and Ahrens T.J. (1993) Planetary cratering mechanics. *J. Geophys. Res.* 98, 17011-17028.

O'Keefe J.D. and Ahrens T.J. (1994) Impact-induced melting of planetary surfaces. In *Large Meteorite Impacts and Planetary Evolution* (eds. B.O. Dressler, R.A.F. Grieve and V.L. Sharpton), GSA Spec. Paper 293, pp. 103-109. Geological Society of America, Boulder, CO.

O'Keefe J.D. and Ahrens T.J. (1996) Planetary strength, central peak oscillation, and formation of complex craters (abstract). *Lunar Planet. Sci. XXVII*, 983-984.

Orphal D.L., Borden W.F., Larson S.A. and Schultz P.H. (1980) Impact melt generation and transport. *Proc. Lunar Planet. Sci. Conf. 11th*, 2309-2323.

Pierazzo E., Vickery A.M., and Melosh H.J. (1997) A re-evaluation of impact melt production. *Icarus*, in press.

Pieters C.M., Tompkins S., He G., Head J.W. and Hess P.C. (1997) Mineralogy of the mafic anomaly at South Pole-Aitken and implications for mantle excavation (abstract). *Lunar Planet. Sci. XXVIII*, 1113-1114.

Pike R.J. (1974) Depth/diameter relations of fresh lunar craters: Revision from spacecraft data. *Geophys. Res. Lett.* **1**, 291-294.

Pike R.J. (1980) Geometric interpretation of lunar craters. U.S. Geological Survey Professional Paper, 77pp.

Pike R.J. (1988) Geomorphology of impact craters on Mercury. In *Mercury* (eds. F. Vilas, C.R. Chapman and M.S. Matthews), pp. 165-273. University of Arizona Press, Tucson.

Quaide W.L. and Oberbeck V.R. (1968) Thickness determinations of the lunar surface layer from lunar impact craters. *J. Geophys. Res.* **73**, 5247-5270.

Redeker H.-J. and Stöffler D. (1988) The allochthonous polymict breccia layer of the Haughton impact crater, Devon Island, Canada. *Meteoritics* **23**, 185-196.

Rockow K.M. and Haskin L.A. (1996) Why are Apollo 17 impact melt breccias assigned a Serenitatis origin: A brief critical review (abstract). *Lunar Planet. Sci. XXVII*, 1089-1090.

Roddy D.J., Pepin R.O. and Merrill R.B. (1977) *Impact and Explosion Cratering*, Pergamon Press, New York 1301pp.

Ruoff A.L. (1967) Linear shock-velocity-particle-velocity relationship. *J. Appl. Phys.* **38**, 4976-4980.

Ryder G., Norman M.D. and Taylor G.J. (1997) The complex stratigraphy of the highland crust in the Serenitatis region of the Moon inferred from mineral fragment chemistry. *Geochim.Cosmochim.Acta* **61**(1083-1105).

Schmidt R.M. (1980) Meteor Crater: Energy of formation -- implications of centrifuge scaling. *Proc. Lunar Planet. Sci. Conf. 11th*, 2099-2128.

Schmidt R.M. and Housen K.R. (1987) Some recent advances in the scaling of impact and explosion cratering. *Internat. J. Impact Engin.* **5**, 543-560.

Schultz P.H. (1976) *Moon Morphology*. University of Texas Press, Austin, TX. 626pp.

Schultz P.H. (1988) Cratering on Mercury: A relook. In *Mercury* (eds. F. Vilas, C. R. Chapman and M. S. Matthews), pp. 274-335. University of Arizona Press, Tucson, AZ.

Settle M. and Head J.W., III. (1979) The role of rim slumping in the modification of lunar impact craters. *J. Geophys. Res.* **84**, 3081-3096.

Shoemaker E.M. (1963) Impact mechanics at Meteor Crater, Arizona. In *The Solar System. IV. The Moon, Meteorites, and Comets* (eds. B.M. Middlehurst and G.P. Kuiper), pp. 301-336. The University of Chicago Press, Chicago.

Shoemaker E.M. (1977) Astronomically observable crater-forming projectiles. In *Impact and Explosion Cratering* (eds. D.J. Roddy, R.O. Pepin and R.B. Merrill), pp. 617-628. Pergamon Press, New York.

Shoemaker E.M. and Wolfe R.F. (1987) Crater production on Venus and Earth by asteroid and comet impact (abstract). *Lunar Planet. Sci. XVIII*, 918-919.

Simonds C.H., Floran R.J., McGee P.E., Phinney W.C. and Warner J.L. (1978) Petrogenesis of melt rocks, Manicouagan impact structure, Quebec. *J. Geophys. Res.* **83**, 2773-2788.

Simonds C.H., Warner J.L. and Phinney W.C. (1976a) Thermal regimes in cratered terrain with emphasis on the role of impact melt. *Amer. Mineral.* **61**, 569-577.

Simonds C.H., Warner J.L., Phinney W.C. and McGee P.E. (1976b) Thermal model for impact breccia lithification: Manicouagan and the Moon. *Proc. Lunar Sci. Conf. 7th*, 2509-2528.

Smith E.I. and Sanchez A.G. (1973) Fresh lunar craters: Morphology as a function of diameter, a possible criterion for crater origin. *Modern Geol.* **4**, 51-59.

Spudis P.D. (1978) Comporition and origin of the Apennine Bench Formation. *Proc. Lunar Planet. SCi. Conf. 9th*, 3379-3394.

Spudis P.D. (1993) *The Geology of Multi-Ring Impact Basins: The Moon and Other Planets*. Cambridge University Press, Cambridge, UK. 263pp.

Spudis P.D., Hawke B.R. and Lucey P.G. (1984) Composition of Orientale Basin deposits and implications for the lunar basin-forming process. *Proc. Lunar Planet. Sci. Conf. 15th*, in *Jour. Geophys. Res.*, **89**, C197-C210.

Spudis P.D. and Ryder G. (1981) Apollo 17 impact melts and their relation to the Serenitatis basin. In *Multi-ring Basins, Proc. Lunar Planet. Sci. Conf. 12A*, 133-148.

Stöffler D., Knöll H.-D., Marvin U.B., Simonds C.H. and Warren P.H. (1980) Recommended classification and nomenclature of lunar highland rocks -- a committee report. In *Proceedings of the Conference on the Lunar Highlands Crust* (eds. J. J. Papike and R. B. Merrill), pp. 51-70. Pergamon, New York.

Stöffler D., Brockmeyer P., Buhl D., Lakomy R., Müller-Mohr V. (1994) The formation of the Sudbury Structure, Canada: Toward a unified impact model. In *Large Meteorite Impacts and Planetary Evolution* (eds. B.O. Dressler, R.A.F. Grieve and V.L. Sharpton), GSA Spec. Paper 293, pp. 303-318. Geological Society of America, Boulder, CO.

Taylor G. J., Warren P. H., Ryder G., Delano J. W., Pieters C. M. and Lofgren G. E. (1991) Lunar Rocks. In *Lunar Sourcebook: A User's Guide to the Moon* (eds. G. H. Heiken, D. T. Vaniman and B. M. French), pp. 183-284. Cambridge University Press, New York.

Tonks W.B. and Melosh H.J. (1992) Core formation by giant impacts. *Icarus* **100**, 326-346.

Tonks W.B. and Melosh H.J. (1993) Magma ocean formation due to giant impacts. *Journal of Geophysical Research* **98**, 5319-5333.

Warren P.H., Claeys P. and Cedillo-Pardo E. (1996) Mega-impact melt petrology (Chicxulub, Sudbury, and the Moon): Effects of scale and other factors on potential for fractional crystallization and

development of cumulates. In The Cretaceous-Tertiary Event and Other Catastrophes in Earth History (Eds. G. Ryder, D. Fastovsky, and S. Gartner), GSA Spec. Paper 307, pp. 105-124. Geol. Soc. Amer., Boulder, CO.

Wilhelms D.E. (1987) *The Geologic History of the Moon*, 327 pp.. U.S. Geological Survey.

Zuber M.T., Smith D.E., Lemoine F.G. and Neumann G. A. (1994) The shape and internal structure of the Moon from the Clementine Mission. *Science* **266**, 1839-1843.